Fabrication and Characterization of Novel Crosslinked Composite Membranes for Direct Methanol Fuel Cell Application – Part I. Poly (Vinyl Alcohol-Co-Vinyl Acetate-Co-Itaconic Acid)/ Phosphotungstic Acid Based Membranes

Arfat Anis[1,2,], S. M. Al-Zahrani[1], A.K. Banthia[2] and S. Bandyopadhyay[3]*

[1] Department of Chemical Engineering, King Saud University, P.O. Box - 800, Riyadh 11421, Saudi Arabia
[2] Materials Science Centre, Indian Institute of Technology, Kharagpur, India - 721302
[3] School of Materials Science & Engineering, University of New South Wales, Sydney 2052, Australia
[*]E-mail: anisarfat@yahoo.co.in

A series of novel cross-linked Poly (vinyl alcohol-co-vinyl acetate-co-itaconic acid) (PVACO) and phosphotungstic acid (PTA) based organic-inorganic composite membranes have been prepared and characterized for direct methanol fuel cell (DMFC) applications. The characteristic properties of these crosslinked composite membranes were investigated by Fourier transform infrared spectroscopy (FTIR), thermogravimetric analysis (TGA), X-ray diffraction (XRD), Atomic Force Microscopy (AFM), methanol permeability measurement and AC impedance spectroscopy. The ionic conductivity of the membranes were investigated as a function of PTA composition, crosslinking density and temperature, were in the order of 10^{-3} S/cm. The methanol permeability of PVACO/PTA composite membranes were in the order of 10^{-6} cm^2/s. The membrane with the best selectivity was found to have a conductivity of 2.3 x 10^{-3} S/cm and a methanol permeability of 3.35×10^{-6} cm^2/s. These membranes showed an Arrhenius behavior for the variation in conductivity with temperature and their activation energies were in the range of 0.13 -0.17 eV.

1. INTRODUCTION

Recent technologies have led more efficient use of electrical energy however still the demand for electrical energy is the growing at an unprecedented pace. One of the major challenges that confront the electricity industry is to address the public concern associated with the environmental

impact of emissions from electricity generation and use. Fuel Cells in general offer an attractive and innovative alternative to current power sources with better efficiencies, renewable fuels and low environmental impact.

Direct methanol fuel cells (DMFCs), in particular, have generated enormous research interest as one of the most potential power source for stationary and portable applications. DMFCs are an attractive power source owing to their high energy density compared to current lithium ion rechargeable batteries and low pollutant emission [1]. DMFC uses liquid methanol as fuel which can be easily adapted with the existing fuel infrastructure for its transportation and storage. At present the most widely used polymer electrolyte membrane in DMFCs is Nafion® membrane commercially produced by DuPont. However large scale commercialization of the DMFCs has been restricted due to several associated technological problems such as slow methanol oxidation kinetics, catalyst poisoning and high methanol crossover associated with the currently used Nafion membranes. The fuel crossover from anode to the cathode through the currently used Nafion membrane causes mixed potential at the cathode which severely degrades the electrochemical performance of the DMFCs. Widespread use of Nafion is also a cause of environmental concern due to the fluorine chemistry involved in its preparation. Thus it is imperative to develop a PEM with much better methanol resistance than Nafion to improve the electrochemical performance of these fuel cells.

Composite membranes can be a promising alternative to the commercially available perfluorosulfonic acid membranes. Recently, Yang et al. [2,3] reported the preparation of a cross-linked PVA/MMT composite polymer membrane for an acidic DMFC. However the performance of such hybrid membranes employed in fuel cells is not always satisfactory due to bleeding out of the dopant which results in depleted performance with time. Hence, a membrane with an effectively immobilized dopant is required. For this purpose, poly vinyl alcohol and its copolymers appear to be among the promising candidates because of their good chemical stability, film forming ability, high hydrophilicity and availability of crosslinking sites to create a stable membrane with good mechanical properties and selective permeability to water. The functional groups present in PVA and PVACO can interact with the dopant to render them immobile within the polymer matrix. PVA membranes have also been used in alcohol dehydration to break the alcohol-water azeotrope [4,5] and due to its high selectivity for water to alcohol; it can effectively reduce the methanol crossover through the membranes for DMFC applications. Kumar et al. [6] reported poly(vinyl alcohol)/para toluene sulfonic acid (PVA/PTSA) composite membranes and found that the PTSA greatly enhanced the ionic conductivity of PVA/PTSA composite membranes. Rhim et al. [7] synthesized a PVA/sulfosuccinic acid (SSA) proton-conducting polymer membrane which had both sulfonic acid and carboxylic acid groups which served as the cross-linking agent and a proton donor. Some authors [8,9] have studied a sulfonated poly(ether ether ketone)/poly(vinyl alcohol) (SPEEK/PVA) membranes for fuel cell and reported that a sub-layer of the PVA polymer attached itself to the anode and provided a good barrier for the alcohol crossover, whereas the SPEEK sub-layer maintained the mechanical stability and a low swelling ratio. Sahu et al. [10] investigated the effects of poly(styrene sulfonic acid) content on a PVA/PSSA composite membranes and its application in a hydrogen - oxygen PEMFC. They reported that with the optimized PVA/PSSA polymer membrane, the PEMFC achieved a peak power density of

210 mWcm^{-2} at 500 mAcm^{-2} at 75 ^{o}C compared to a peak power density of only 38 mWcm^{-2} at 80 mAcm^{-2} for the PEMFC with a pristine PVA membrane.

Heteropolyacids (HPAs) are a very attractive as inorganic fillers for composite membrane preparation because they are highly conductive and thermally stable in their crystalline form. These acids exist in several hydrated forms depending on the hydration environment [11,12]. In hydrated phase, the HPA molecules are bridged by water molecules to form hydronium ions such as $H_5O_2^+$. Kreuer suggested that the HPA acts as a Bronsted acid toward the water of hydration, which bounds loosely to its structure, resulting in high proton conductivity [13]. Ramani et al. and Herring et al. reported that the addition of HPAs to the perfluorosulfonic acid (PFSA) ionomers leads to improvement in its proton conductivity and durability and it also improves the performance of membrane electrode assemblies (MEAs) [14-17]. Heteropoly acids have also been used to improve the conductivity and thermal stability of the polymer electrolyte membranes [18]. Previously we have reported the properties of crosslinked composite membranes of PVA and it copolymer with phosphomolybdic acid and silicotungtic acid with promising properties for DMFC application [19-21].

Heteropoly acid (HPA) being an inorganic acid catalyses the polymer crosslinking reaction and at the same helps in the oxidation of the methanol fuel [22] and hence can effectively reduce the crossover of methanol. To overcome the leakage problem of the HPA from the membrane and hence maintain the proton conductivity of the membranes, they are immobilized in polymer matrix by in situ chemical crosslinking of the polymer matrix to form crosslinked networks.

The present work reports the fabrication and characterization of low cost, environment friendly proton conducting composite polymer electrolyte membranes with potential for DMFC application. An environment friendly, biodegradable copolymer of PVA namely Poly (vinyl alcohol-co-vinyl acetate-co-itaconic acid) (PVACO) has been utilized as the polymer matrix and phosphotungstic (PTA), a heteropolyacid as the dopant for the preparation of chemically crosslinked composite polymer electrolyte membranes. The prepared composite polymer electrolyte membranes have been characterized by various characterization techniques to study their feasibility as possible alternative proton conducting polymer electrolyte membranes for DMFC application.

2. EXPERIMENTAL

2.1. Preparation of the PVACO-PTA composite membrane

Poly (vinyl alcohol-co-vinyl acetate-co-itaconic acid), degree of hydrolysis approx. 97 mole % was obtained from Aldrich, USA. Phosphotungstic Acid was obtained from Sisco Research Laboratories (SRL) Pvt. Ltd., Mumbai, India. Glutaraldehyde (25 % aqueous solution) was obtained from LOBA Chemie Pvt. Ltd., Mumbai, India and was diluted to 5 % aqueous solution before being used in the preparation of these composite PEMs, Methanol was obtained from Merck Limited, Mumbai, India. The PVACO-PTA crosslinked composite membranes were prepared by a solution casting method. The polymer solution (5 % (w/v)) was prepared by dissolving PVACO in deionized water at 80 ^{o}C with continuous stirring until homogeneous and viscous. The required amount of the

PTA was added to 20 g of the 5 wt % polymer solution and the resulting mixture was stirred at room temperature (25 ^{o}C) until a homogeneous solution was obtained. The required amount of the glutaraldehyde (GA) crosslinking reagent (CLR) was added to the PVACO-PTA homogeneous solution and the solution was further stirred for a few minutes to homogenize the solution for accomplishing uniform crosslinking. After this, the solution was poured onto glass petridish and allowed to dry at room temperature for around 48 hours. The dried membranes were peeled off the glass substrate and the obtained membranes were approximately 100 ±10 μm in thickness.

2.2. FTIR Spectroscopy, Water Uptake and Dopant Loss Measurements

Attenuated Total Reflection (ATR)-FTIR spectra of the pure polymer membranes, pure heteropoly acids and the composite membranes was obtained with a FTIR Spectroscope (NEXUS-870, Thermo Nicolet Corporation) in the range of 4000 - 600 cm^{-1} using Omnic Software maintaining a uniform resolution of 2 cm^{-1} during the collection of the spectral data. Water uptake of the crosslinked pristine polymer membranes and the composite membranes was determined by measuring the change in the weight before and after hydration.

The membranes were equilibrated in deionized water for 24 hours at 25 ^{o}C, and the surface attached water on the membrane was removed carefully by placing both the surfaces of the membranes gently over a filter paper. The weight of the wetted membrane was determined quickly using an analytical balance with a sensitivity of 0.1 mg. Water uptake was calculated by using the following equation:

$$Water \quad uptake = \frac{M_w - M_d}{M_d}$$

where M_w and M_d is the weight of the wetted polymer and dry polymer membranes in grams respectively.

Titration method was used to determine the dopant loss from the membranes due to bleeding out of the PTAs upon hydration. The composite membranes were equilibrated in 50 ml of deionized water for 24 hours at ambient temperature (25 ^{o}C). Then, 10 ml of the solution was titrated with standardized 0.01 N NaOH solution. The dopant loss was calculated by using the following equation:

$$DL = \frac{A \ x \ 0.01 \ x \ 5}{m}$$

where *DL* is the dopant loss (meq./g), *A* the NaOH used to neutralize the resulting aqueous solution after equilibration (ml), 0.01 the normality of the NaOH, 5 the factor corresponding to the ratio of the amount of water taken to equilibrate the polymer to the amount used for titration, and *m* the sample mass (g).

2.3. Impedance Spectroscopy and Methanol Permeability Measurements

Conductivity measurements for the PVACO-PTA composite membranes were made via the AC impedance method. The PVACO-PTA composite membranes were first equilibrated in deionized water for 24 h at room temperature (25 ^{o}C). The equilibrated membrane was sandwiched between stainless steel (SS304), ion blocking electrodes, each of surface area 1.72 cm^{2}, in a spring loaded teflon holder with a thermocouple attached close to the electrodes for accurately recording the measurement temperature. The samples were equilibrated at the measurement temperature for 30 minutes before making the measurements and the experimental temperatures were maintained within ±0.5 ◦C during the measurements. AC impedance spectra of the membranes were obtained by using Agilent 4294A Precision Impedance Analyzer under an oscillation potential of 10 mV from 40 Hz to 10 MHz at 100 % relative humidity to prevent any moisture loss from the membrane due to desorption during the measurements [23]. The conductivity was calculated from the bulk resistance obtained from the high frequency intercept of the imaginary component of impedance with the real axis. The conductivity of the membrane is calculated using the following equation:

$$\sigma = \frac{l}{RA}$$

where σ, R , l and A represent membrane conductivity, bulk resistance, membrane thickness and area of the electrode, respectively.

The measurement of methanol diffusion co-efficient through the composite membranes was performed using an in house built diffusion cell having two compartments separated by the membrane situated horizontally. Prior to diffusion co-efficient measurement, the membranes were equilibrated in aqueous methanol solution 50 % v/v for 24 hours and the experiments were carried out at room temperature (25 ^{o}C). The methanol concentration of the receptor compartment was estimated using a differential refractometer (Photal OTSUKA Electronics, DRM-1021); the differential refractometer is highly sensitive to the presence of methanol. The change in refractive index of the diffusion samples were averaged over 52 scans in the differential refractometer to determine the change in refractive index. The methanol diffusion co-efficient for the PEM was calculated using the following equation [24]:

$$D = \frac{lV_{sample}}{At_{exp}} \ln \frac{C_1 - C_{methanol}}{C_2 - C_{methanol}}$$

where D is the methanol diffusion co-efficient, l is the thickness of the membrane, V_{sample} is the volume of the sample solution; A is the cross-section area of membrane and t_{exp} is the time interval during which diffusion occurs, $C_{methanol}$ is concentration of methanol fed in the donor compartment, C_1 is concentration of methanol in receptor compartment at t = 0 and C_2 is the concentration of methanol in the receptor compartment at t = t $_{exp.}$ All the composite membranes were examined at least three times.

2.4. Thermal, Mechanical and Morphological properties

Thermal stability of the composite membranes were studied by thermogravimetric analysis of the pristine polymers and the composite membranes using a NETZSCH TG 209 F1 thermogravimetric analyzer, at a heating rate of 10 ^{o}C/min, with nitrogen flushed at 100 ml/min. The tensile strength measurements of the composite membranes was carried out using Hounsfield H10KS tensile testing machine at a crosshead speed of 12.5 mm/min, temperature 27 ^{o}C and 75 % humidity. The gauge dimension of the dog bone shaped test samples was 5 mm x 50 mm. For each sample, three specimens were tested to determine the average value of tensile strength and percent elongation at break [25]. X-ray diffraction patterns for the pristine raw materials and the composite membranes were obtained by using a Phillips X-Pert Diffractometer, using a Cu-Kα1 radiation and operating at 40 kV and 25 mA. The diffractometer was controlled by a personal computer equipped with X-pert High Score Plus Software. The X-ray diffraction patterns were collected with a scan rate of 4.2 degree/min from $2\theta = 5$ - 50 ^{o}. Atomic force microscopy of the membranes was performed using a Digital Instruments 3000 AFM, controlled by Nanoscope IIIa scanning probe microscope controller with a Nanoprobe Tapping (TESP) SPM tip from Digital Instruments, CA. The tapping tip is mounted on 125 µm long, single beam cantilevers, with resonant frequencies in the range of 330-399 kHz and corresponding spring constants of 20-100 N/m.

3. RESULTS AND DISCUSSION

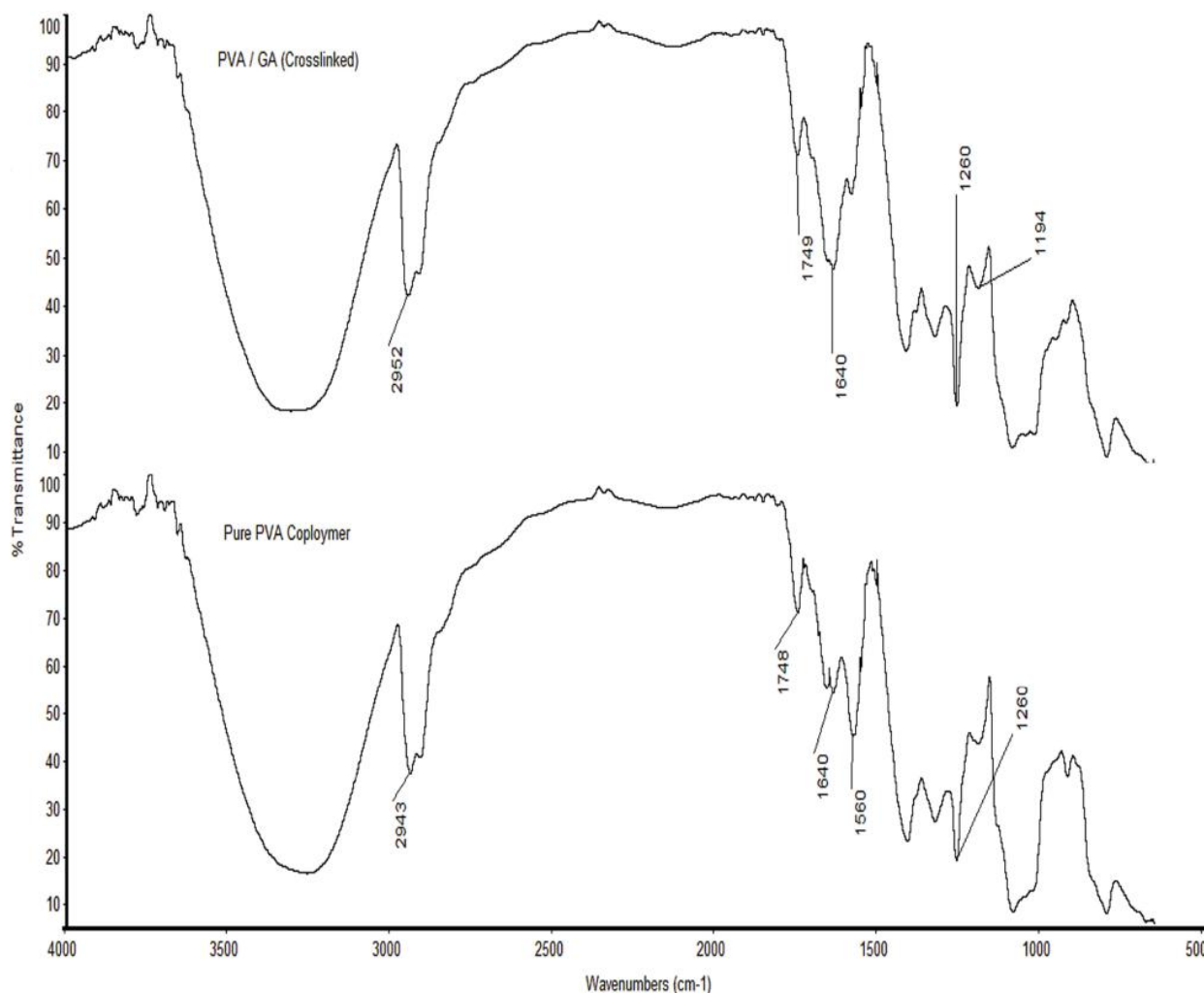*3.1. FTIR Spectroscopy, Water Uptake and Dopant Loss Measurements*

The FTIR spectrum of the Pure PVACO membrane is showed in Fig. 1 and it clearly depicts the major peaks associated with the poly (vinyl alcohol-co-vinyl acetate-co-itaconic acid). The C–H broad alkyl stretching band ($\nu = 2850\text{-}3000$ cm^{-1}) and typical strong hydroxyl bands for hydrogen bonded alcohol ($\nu = 3200\text{-}3570$ cm^{-1}) can be observed in the spectra. Intra-molecular and intermolecular hydrogen bonding are expected to occur among PVACO chains due to high hydrophilic forces. The peak at $\nu = 1640$, 1748 cm^{-1} is due to C=O stretching of saturated aliphatic esters (acetate) and carboxylic acid (itaconic acid), a broad absorption band (from $\nu = 1000$ - 1320 cm^{-1}) is attributed to the (C-O) stretching of alcohol, ester and carboxylic acid groups of the PVACO.

The FTIR spectrum in Fig. 1 also shows the spectra associated with PVACO crosslinked by glutaraldehyde (PVACO/GA). By crosslinking PVACO with GA the intensity of the O-H stretching vibration peak ($\nu = 3200\text{-}3400$ cm^{-1}) decreased and peak frequency shifted from 3262 to 3311 cm^{-1}, i.e. to a higher frequency as compared to that of pure PVACO which confirms the occurrence of the crosslinking reaction at the hydroxyl group sites. The increase in intensity of the peak at $\nu = 1260$ & 1194 cm^{-1} is attributed to the ether (C-O) and the acetal ring (C-O-C) linkage formation by the crosslinking reaction of PVACO with GA. The relative increase of the C=O band at $\nu = 1640$ cm^{-1} indicates that the aldehyde groups of GA did not completely react with O-H groups of PVACO chain
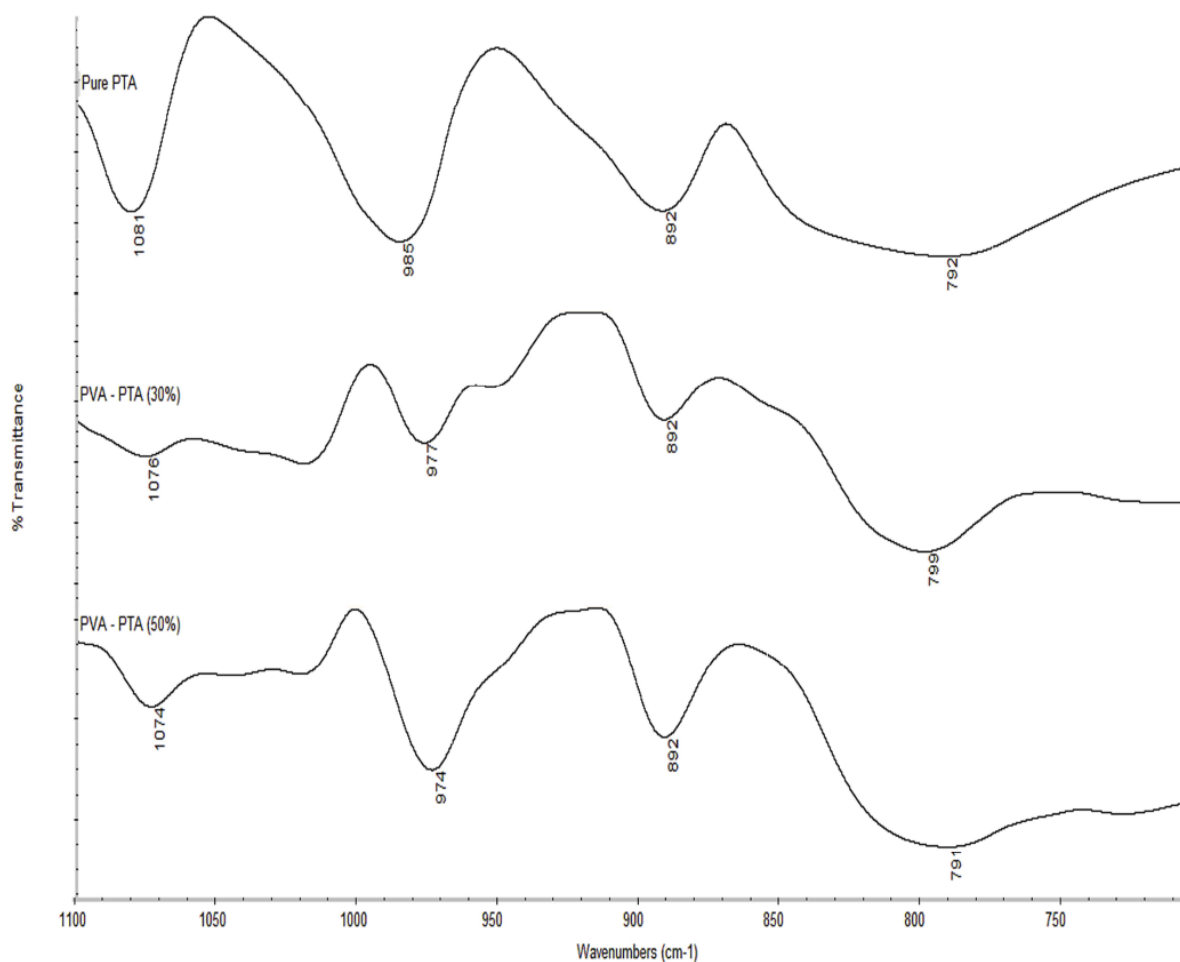
which is due to the absence of an external catalyst, which is generally employed to facilitate this crosslinking reaction.

The FTIR spectra of pure PTA and the influence of PTA addition on the skeletal modes in the PVACO/PTA composites are depicted in Fig. 2. The FTIR spectrum of pure PTA shows the typical features of Keggin anions. According to the assignments of Rocchiccioli - Deltcheff et al. [26], the absorption bands at 1081, 985, 892, 792 cm^{-1} are assigned to the ν (P-O), ν (W-O$_t$) (O$_t$ refers to the terminal oxygen), ν (W-O$_e$-W) (O$_e$ refers to the edge oxygen) and ν (W-O$_c$-W) (O$_c$ refers to the corner oxygen) respectively. All these characteristic bands of PTA are also present in the spectra of the composites, indicating the preservation of Keggin ions geometry inside the polymer composites.

The frequency shifts of (W-O$_t$-W), (W-O$_c$-W) and (W-O$_e$-W) bands are attributed to the strength of the anion - anion interaction which occurs due to the electrostatic repulsion between the PW anions in the crystalline compound. The increase in distance between the neighbouring oxygens of the PW anions results in increased anion – anion interaction which leads to decrease in frequency of the pure stretching (W-O$_t$) band whereas increase in frequency is expected for the other two vibrations bands because of their mixed bend stretching character [26].
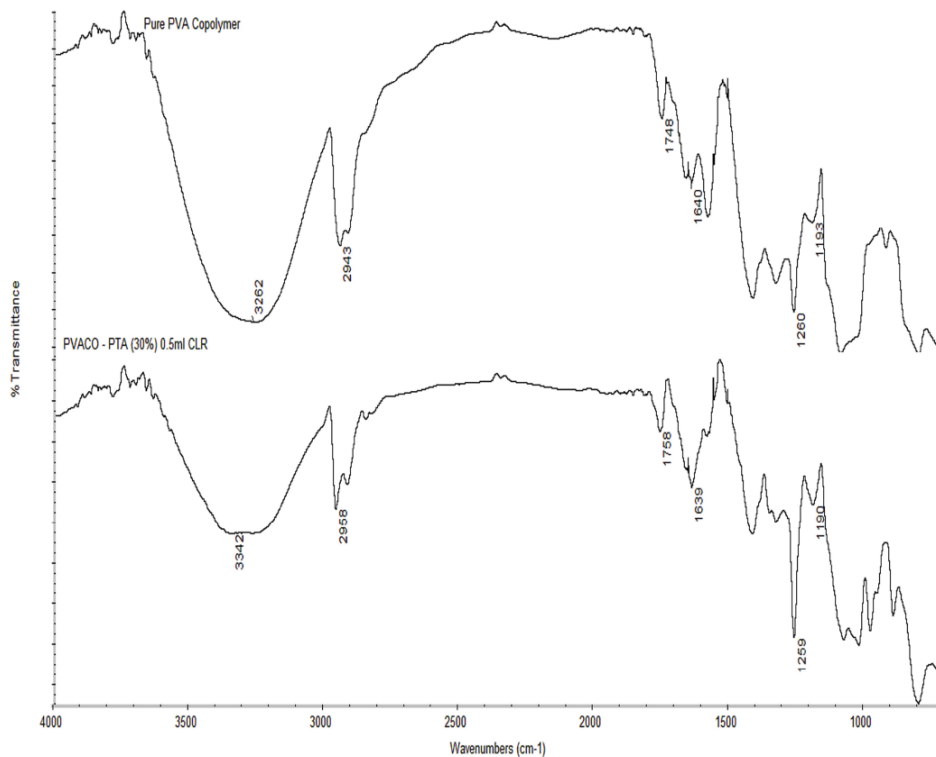

Figure 1. FTIR spectra of Pure PVACO and glutaraldehyde crosslinked Pure PVACO membrane
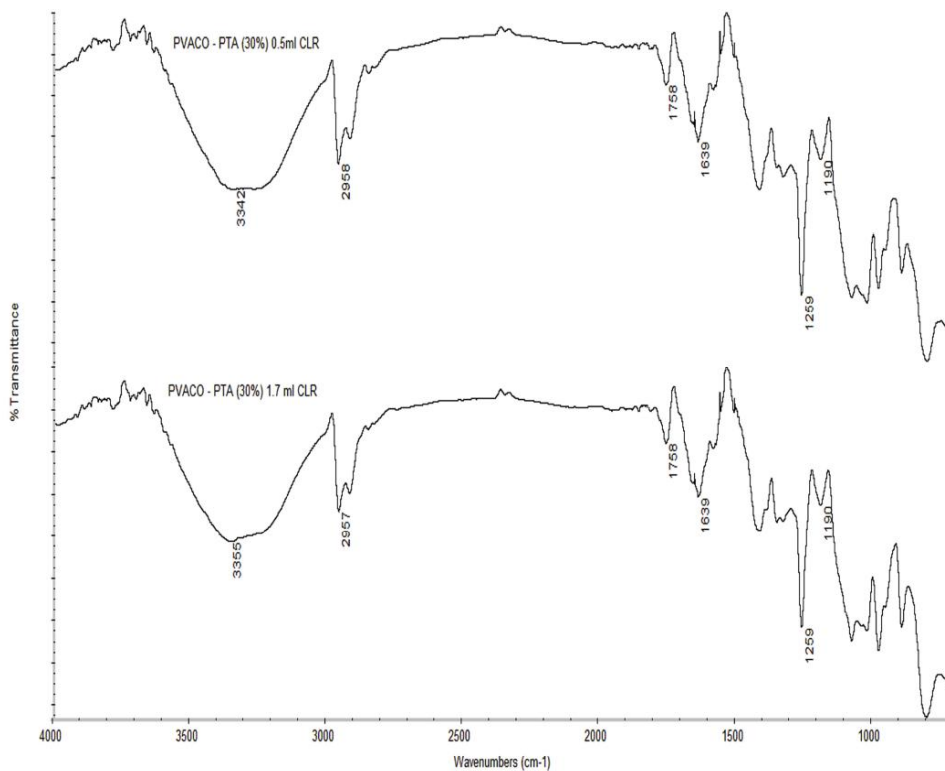
Figure 2. FTIR spectra of Pure PTA and GA crosslinked composite PEMs with different wt. % PTA content and same CLR content (0.5 ml)

The bands ascribed to the ν (P-O) and ν (W-O$_t$) stretching modes move to lower frequencies whereas an increase in frequency is observed for the ν (W-O$_c$-W) stretching vibrations with increase in PTA content of the composite membranes but no change was observed in the position of ν (Mo-O$_e$-Mo) stretching band in the composite membranes. These results clearly show that both the terminal oxygen and the bridging oxygen of PTA interact with the polymer in the composite membranes. Primary interaction occurs through the terminal oxygen and through the corner-shared bridging oxygen in the composite membranes; the edge shared bridging oxygen does not interacts with the polymer as no frequency shift is observed for this band.

The FTIR spectrum in Fig. 3 is associated with PVACO/PTA composite membrane crosslinked by glutaraldehyde. This composite membrane shows a substantial decrease in the O-H stretching vibration peak ($\nu = 3200\text{-}3500$ cm^{-1}) when compared to PVACO/GA membrane without PTA (Fig. 1), a weak peak of the C=O band ($\nu = 1640$ cm^{-1}) indicates that the aldehyde groups of GA have reacted completely with O-H groups of the PVACO chain in the presence of PTA which acts as a catalyst for the PVACO-glutaraldehyde crosslinking reaction. The increase in intensity the C-O stretching peaks at 1260 cm^{-1}, and the frequency shift of the peak at 1193 to 1190 cm^{-1} is attributed to the formation of ether (C-O) and the acetal ring (C-O-C) linkages by the crosslinking reaction of PVACO with GA.
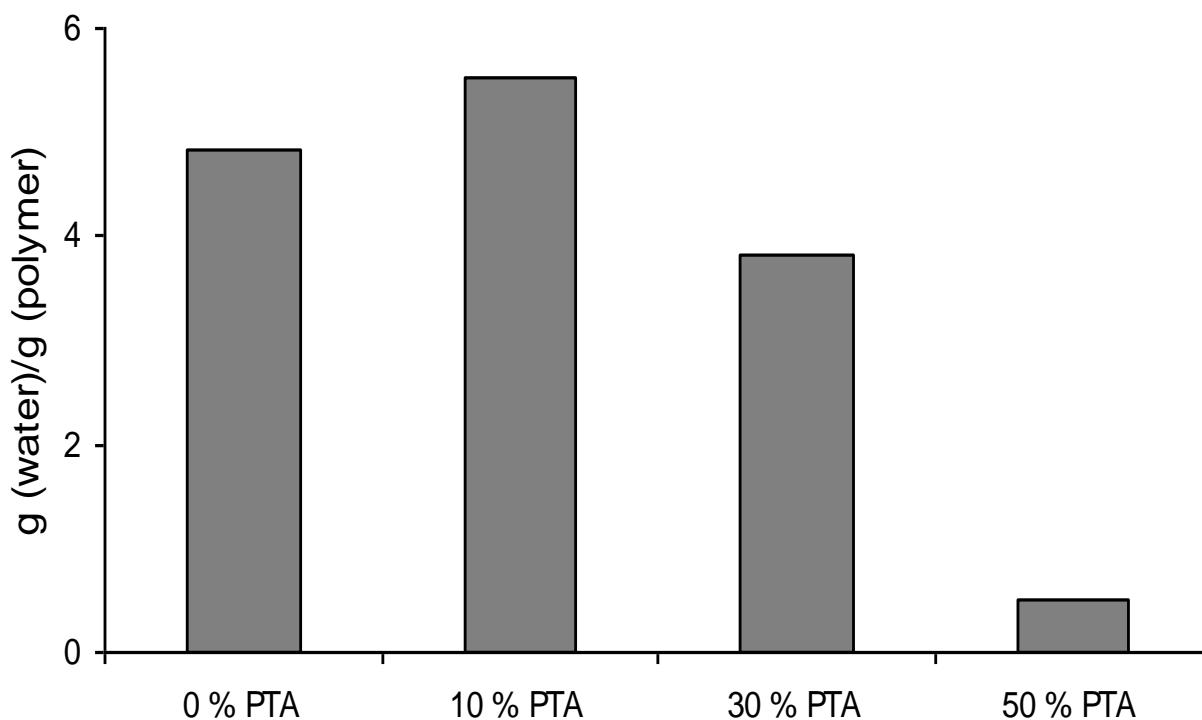
Figure 3. FTIR spectra of Pure PVACO (uncrosslinked) and GA crosslinked (CLR=0.5 ml) composite PEM with 30 wt. % PTA
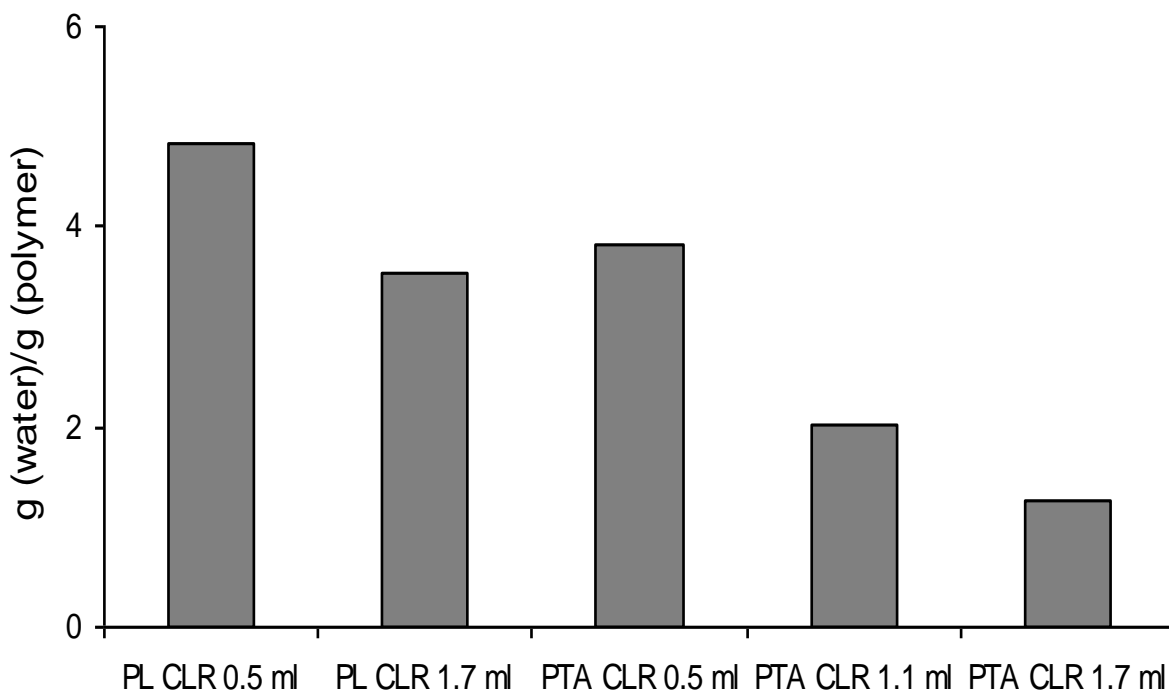

Figure 4. FTIR spectra of crosslinked PVACO/PTA composite PEMs with 30 wt. % PTA & 0.5 & 1.7 ml GA CLR respectively

The FTIR spectra of the PVACO/PTA composite membranes with similar PTA content and different GA CLR contents are depicted in Fig. 4. Further decrease in the O-H stretching vibration peak with increase in CLR content of the composite membranes is observed and an increase in intensity of the peaks associated with the formation of ether (C-O) and the acetal ring (C-O-C) linkages is observed which confirms the accomplishment of the crosslinking reaction in the prepared PVACO/PTA composites.
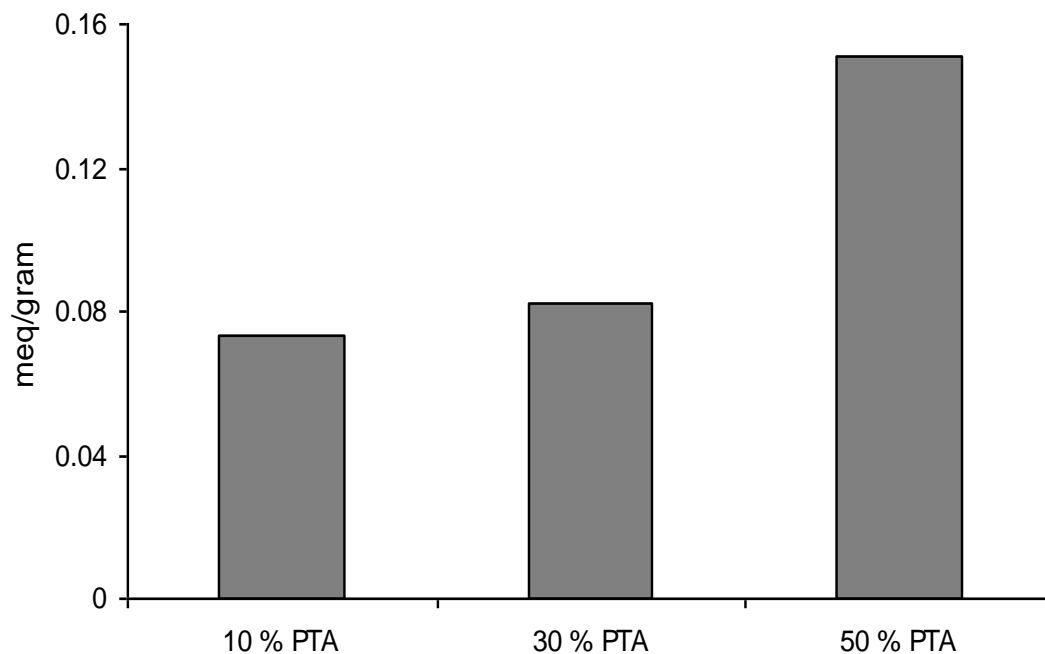
The water uptake of the pristine as well as the PVACO/PTA composite membranes with different wt. % PTA content is showed in Fig. 5. The volume of the glutaraldehyde crosslinking reagent (CLR) used was kept constant (0.5 ml) for the preparation of these composite membranes. The pristine PVACO membrane showed a very high water uptake of 4.8 gram per gram of the dry polymer, an increase of around 15 % in the water uptake of the membrane was observed by the incorporation of 10 wt. % of PTA in the membrane this increase is due to the hydrophilic nature of the PTA. When the PTA content of the membranes was increased to 30 wt. %, 30 % decrease in the water uptake of the composite membrane was observed and with further increase in the PTA content of the composite membranes to 50 wt. %, 85 % decrease in water uptake of the membrane was observed. This decrease in water uptake of the membranes with increasing PTA content is due to the resistance offered by the crosslinked networks, which restrict the swelling and hence the water uptake of the polymer matrix and very well control the hydrophilic character of the composite membranes.

Figure 5. Water Uptake of Crosslinked PVACO membrane & PEMs with different wt. % PTA & 0.5 ml GA CLR
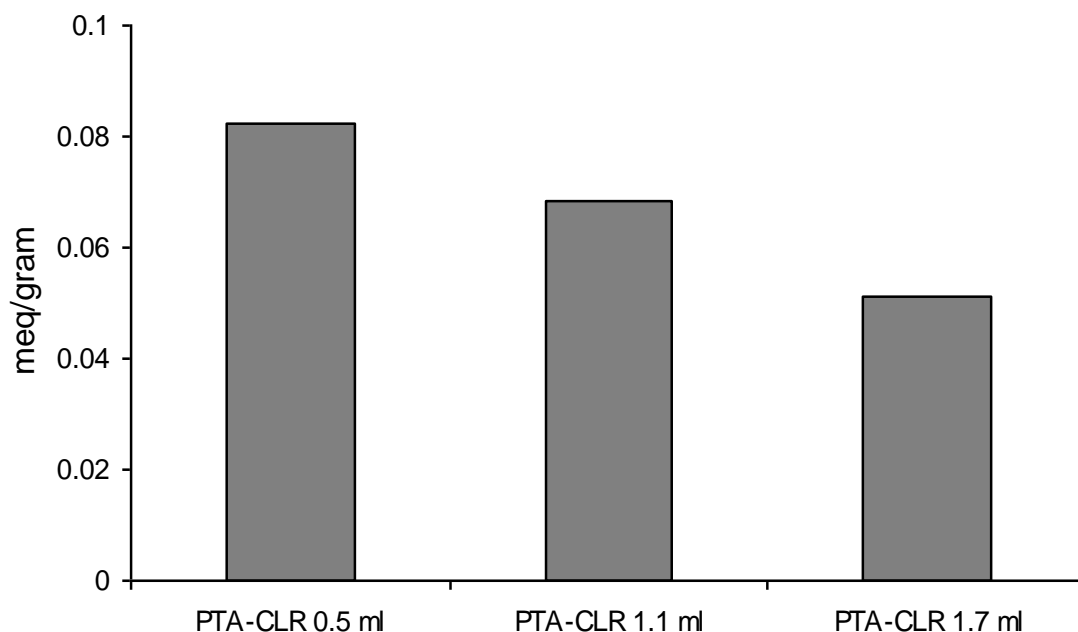
Figure 6. Water Uptake of Crosslinked PVACO (No PTA) and crosslinked PEMs (30 wt. % PTA) with different GA CLR content

Figure 7. Dopant loss from the crosslinked PVACO-PTA composite membranes with (0.5 ml CLR) and different wt. % PTA content

The water uptake of the pristine and the PVACO/PTA composite membranes (30 wt. % PTA content) with different amount of GA CLR content is shown in Fig. 6. The water uptake of the PVACO (without PTA) decreases with increase in the crosslink density of the membrane. A water uptake of 3.8 g/g is observed for the composite membrane with 30 wt. % PTA content that further decreases with increase in cross link density of the membranes. The minimum water uptake of 1.26 g/g is observed for the composite membranes with 30 wt. % PTA content and 1.7 ml of GA CLR content.

The loss of dopant from the polymer matrix is one the major problem associated with composite polymer electrolyte membranes which leads to loss in performance of the membrane with time. The dopant loss values for the PVACO/PTA composite membranes are plotted as a function of wt. % PTA content and GA CLR content of the membranes in Fig. 7 and 8 respectively. It can be seen that the dopant loss from the composite membranes increases with increase in PTA content of the membrane. To enhance the immobilization of the PTA in the composite membranes the crosslink density of the membranes was increased. A decrease in the dopant loss from the crosslinked composite membranes was observed that with increase in crosslink density of the composite membranes.
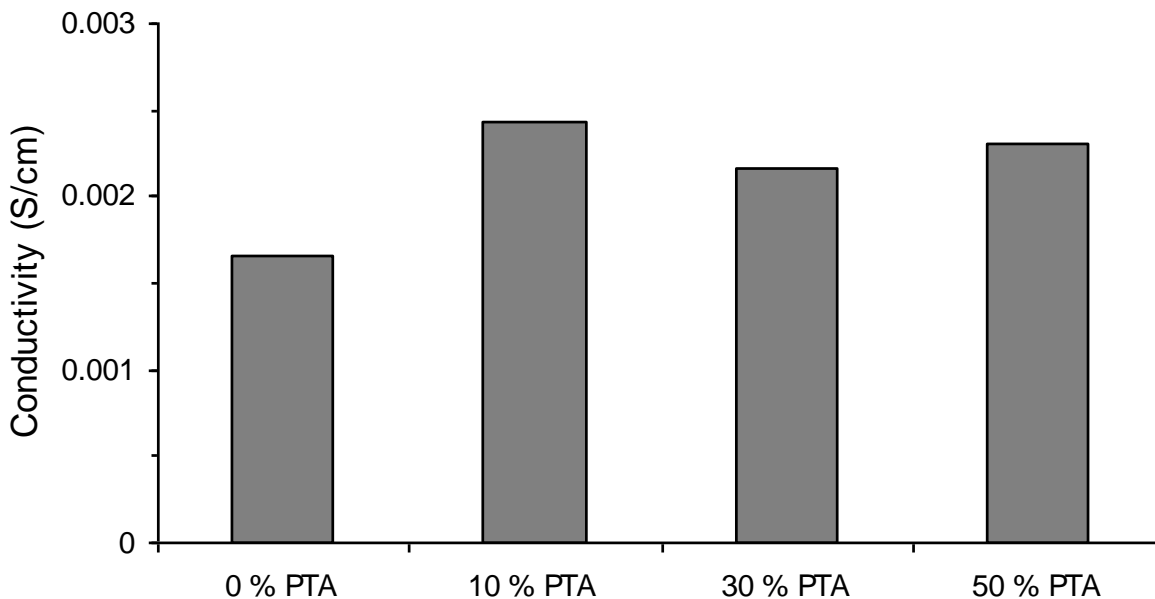

Figure 8. Dopant loss from the crosslinked PVACO-PTA composites with 30 wt. % PTA and different amount of GA CLR content
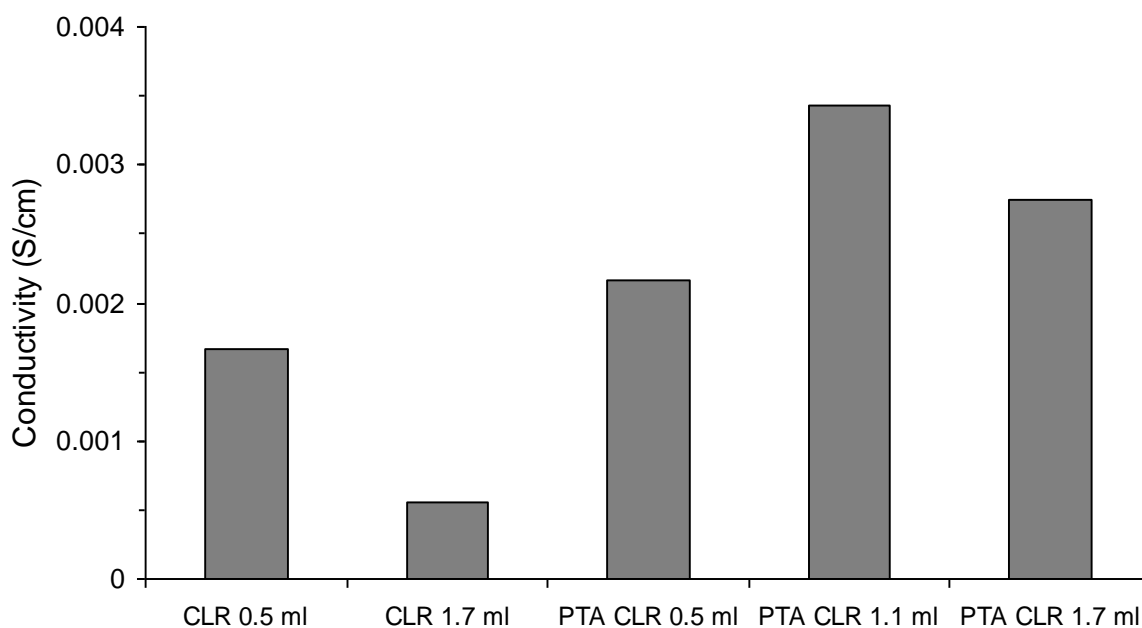
3.3. Proton Conductivity and Methanol Permeability Measurements

The proton conductivity values for the cross-linked pristine PVACO membrane as well as the PVACO/PTA composite membranes with different wt. % PTA content are shown in Fig. 9. The conductivity of the PVACO/PTA composite membranes increases with the incorporation of 10 wt. %

PTA, but slight decrease in conductivity is observed with further increase PTA content of the membranes.
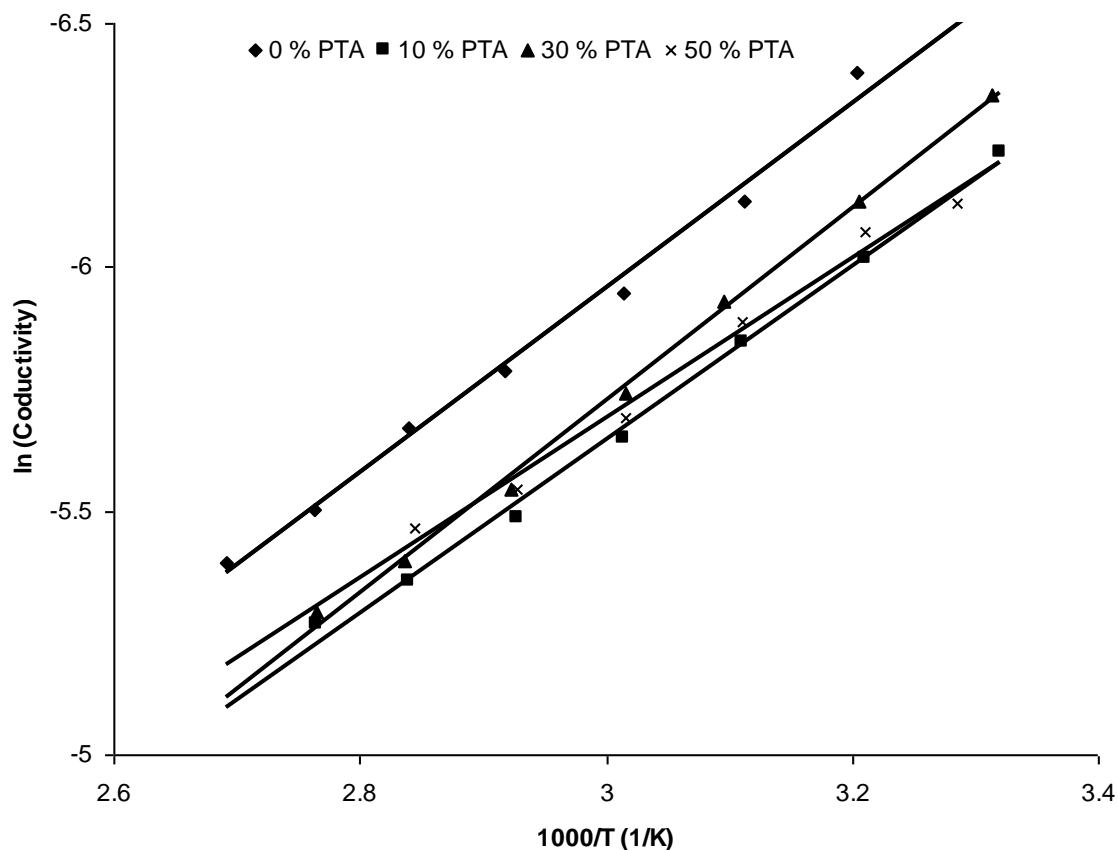

Figure 9. Conductivity of Crosslinked PVACO membrane (No PTA) & crosslinked composite PEMs with different wt. % PTA & 0.5 ml GA CLR
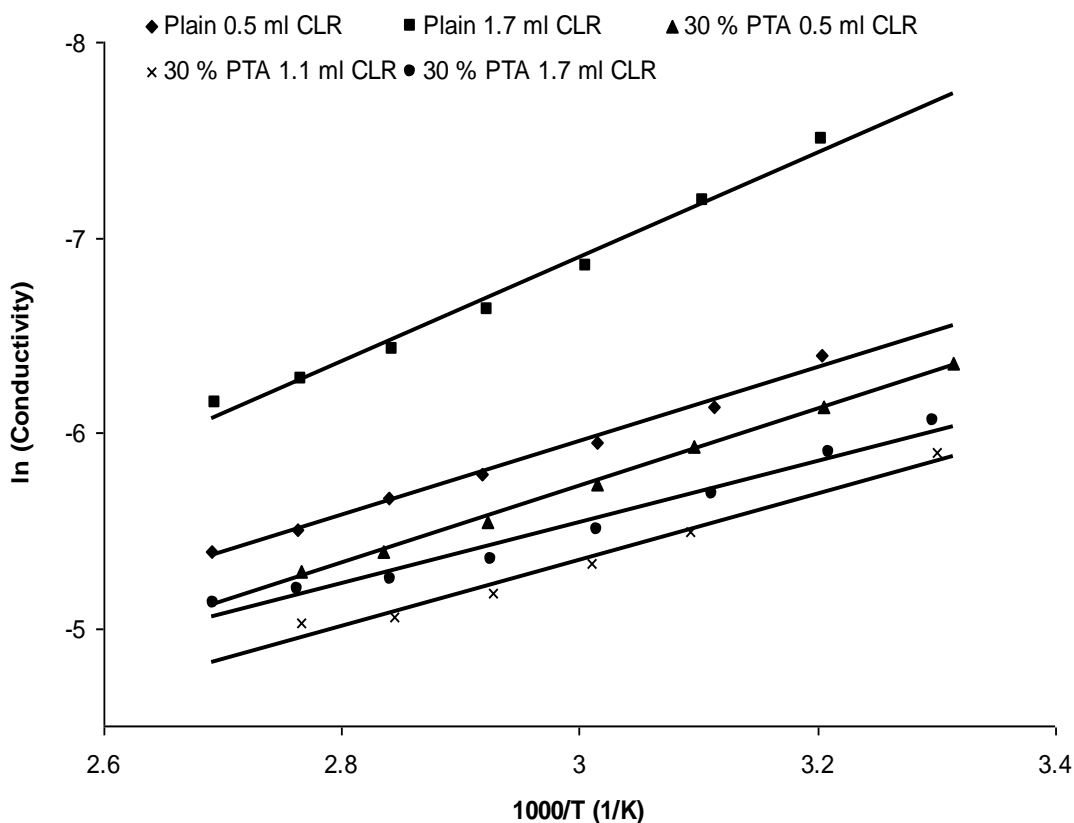

Figure 10. Conductivity of Crosslinked PVACO (No PTA) & crosslinked composite PEMs (30 wt. % PTA) with different amount of GA CLR

The change in conductivity with increase in crosslink density of the pristine as well as the PVACO/PTA composite membranes is shown in Fig. 10. The conductivity of the crosslinked pristine PVACO membrane decreases with increase in crosslink density of the membrane due to decrease in water uptake of the membrane. The conductivity of the PVACO/PTA composite membranes initially increases with increase in crosslink density of the composite membrane but then decreases slightly with further increase in crosslink density which can be attributed to the low water uptake of the membrane at high crosslink density. Recently, Gao et al. [27] have also reported proton conductivity of polyvinyl alcohol/phosphotungtic acid polymer electrolytes in the order of 10^{-3} S/cm. Similar result have also been reported by Guhan et al. [28] for composite membranes with PVA, SPEEK and /phosphotungstic acid and Thanganathan et al. [29] for PVA, poly(tetremethylene oxide), phosphotungstic acid composite membranes.

The variation of conductivity with temperature follows different types of equations according to different kinds of proton-transport mechanism. Arrhenius Eq. can be used to explain the proton hopping mechanism. Fig. 11 and Fig. 12 show the conductivity of the PVACO/PTA composites against the reciprocal absolute temperature, the linear relationship confirms that the variation in conductivity with temperature follows an Arrhenius behavior.

Figure 11. Arrhenius plots for Crosslinked PVACO (No PTA) and crosslinked composite PEMs with different wt. % PTA & 0.5 ml GA CLR

Figure 12. Arrhenius plots for Crosslinked PVACO (No PTA) and the crosslinked composite PEMs with 30 wt. % PTA & different amount of GA CLR

Table 1. R-Squared and Activation Energy values for the Arrhenius plots of the Crosslinked Pure PVACO membranes and the PVACO/PTA crosslinked composite membranes
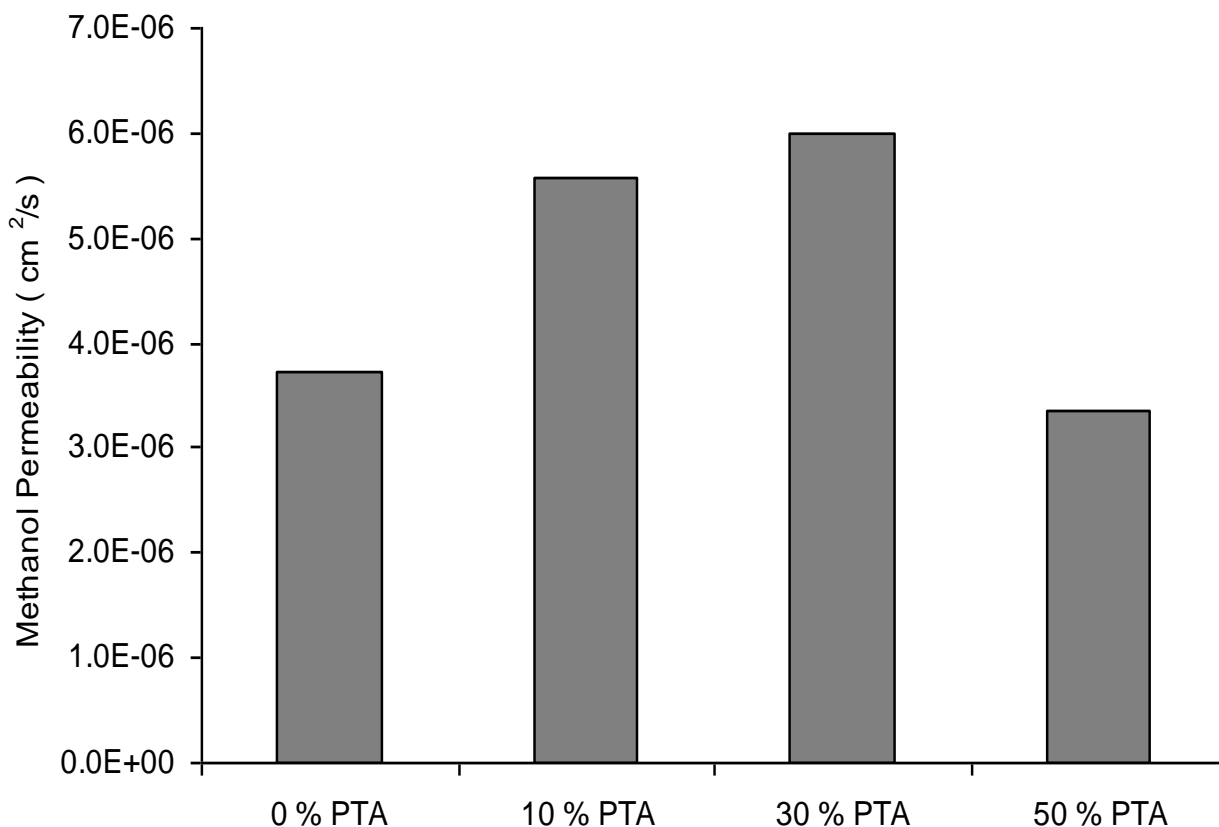
Membrane Details	R^2 Value (line fitting)	Activation Energy (eV)
PVACO / 0 wt. % PTA / CLR 0.5 ml	0.99	0.16
PVACO / 0 wt. % PTA / CLR 1.7 ml	0.98	0.23
PVACO / 10 wt. % PTA / CLR 0.5 ml	0.99	0.15
PVACO / 30 wt. % PTA / CLR 0.5 ml	0.99	0.17
PVACO / 30 wt. % PTA / CLR 1.1 ml	0.98	0.15
PVACO / 30 wt. % PTA / CLR 1.7 ml	0.97	0.13
PVACO / 50 wt. % PTA / CLR 0.5 ml	0.98	0.14

For the crosslinked composite membranes with different wt. % PTA content, the activation energy (Table 1) was initially found to increase from 0.15 eV for 10 wt. % PTA content to 0.17 eV for 30 wt. % PTA content but with further increase in the PTA content the activation energy decreased to 0.14 eV for the composite membranes with 50 wt. % PTA content. For the composite membranes with
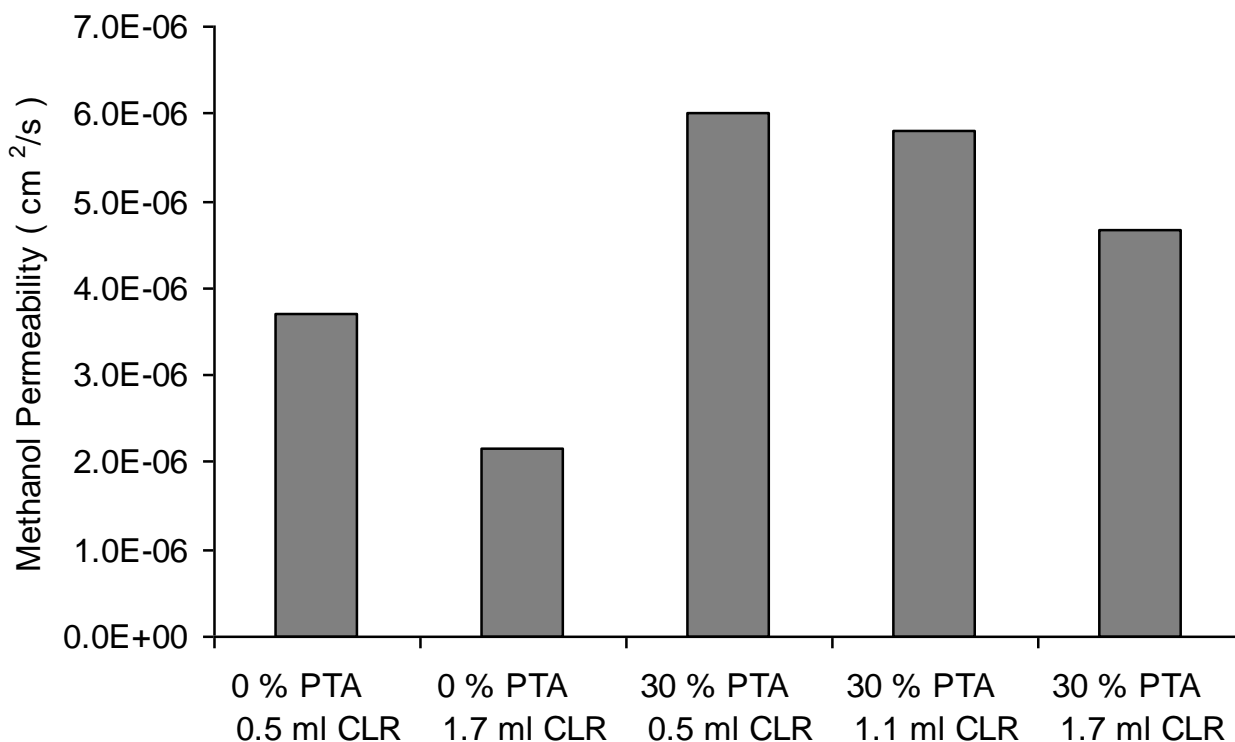
30 wt. % PTA content and different CLR content, the activation energy was found to decrease from 0.17 eV to 0.13 eV with increase in CLR from 0.5 ml to 1.7 ml.

The variation of conductivity with temperature for all the PVACO/PTA composites follow Arrhenius behavior, similar results were also observed for crosslinked PVA/PTA composites [30], therefore it can be confidently proposed that in the studied temperature range the conductivity follows the hopping mechanism. However, the conduction mechanism in the composites is different from that occurring in the pure phosphotungstic acid because the values of the activation energy for the composites are much higher than that for pure PTA.

The methanol permeability of the PVACO/PTA composite membranes with different PTA content is shown in Fig. 13. The pristine PVACO membrane showed lower methanol permeability compared to the composite membranes with different PTA content. The methanol permeability of the composite membranes increases with increase in PTA content of the membrane. With further increase in the PTA content of the composite membranes to 50 wt. % a sharp decrease in methanol permeability of the membrane was observed, this sharp decrease may be attributed to the very low water uptake of this particular composite membrane.

Figure 13. Methanol permeability of Crosslinked PVACO (No PTA) & composite PEMs with different wt. % PTA & 0.5 ml GA CLR
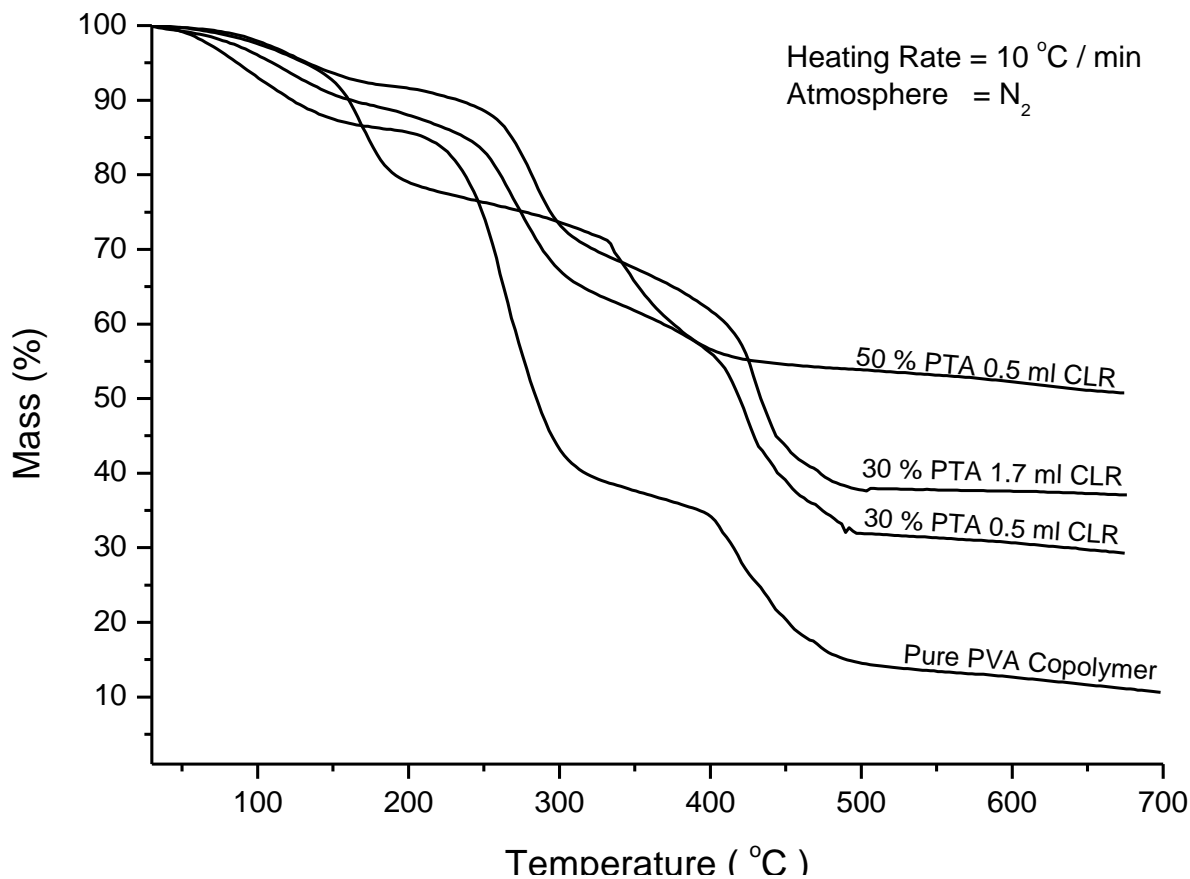
Figure 14. Methanol permeability of Crosslinked PVACO (0 wt % PTA) & composite PEMs with 30 wt. % PTA) & with different amount of GA CLR

Fig. 14 shows the methanol permeability of the PVACO/PTA composite membranes (30 % PTA content) with different CLR content. The methanol permeability of the PVACO membrane (without PTA) decreases with increase in the crosslink density of the membrane. A slight decrease in methanol permeability is observed for the composite membrane with increasing crosslink density but the overall methanol permeability was always greater than that for the crosslinked pristine PVACO membranes. Zhang et al. [31] have also reported similar methanol permeability in the order of 10^{-6} cm^2/s for Nafion® ionomer-implanted PVA/CS composite membranes.

3.4. Thermal, Mechanical and Morphological properties

The thermal stability of the PVACO/PTA composite membranes with different PTA content and crosslink density was investigated by thermo gravimetric analysis. The TGA thermograms of pristine PVACO and PVACO/PTA are showed in Fig. 15. The pristine PVACO is thermally stable up to 230 ^{o}C. Three consecutive weight loss steps are observed for the PVACO/PTA composite membranes, the corresponding percentage weight loss is reported in Table 2. Each weight loss step is responsible for a thermal solvation, thermal degradation of the cross links (ester and ether linkages) and finally a thermal oxidation of the polymer chain respectively. The PVACO/PTA composite membranes show enhanced thermal stability and the composite membrane shows first major weight
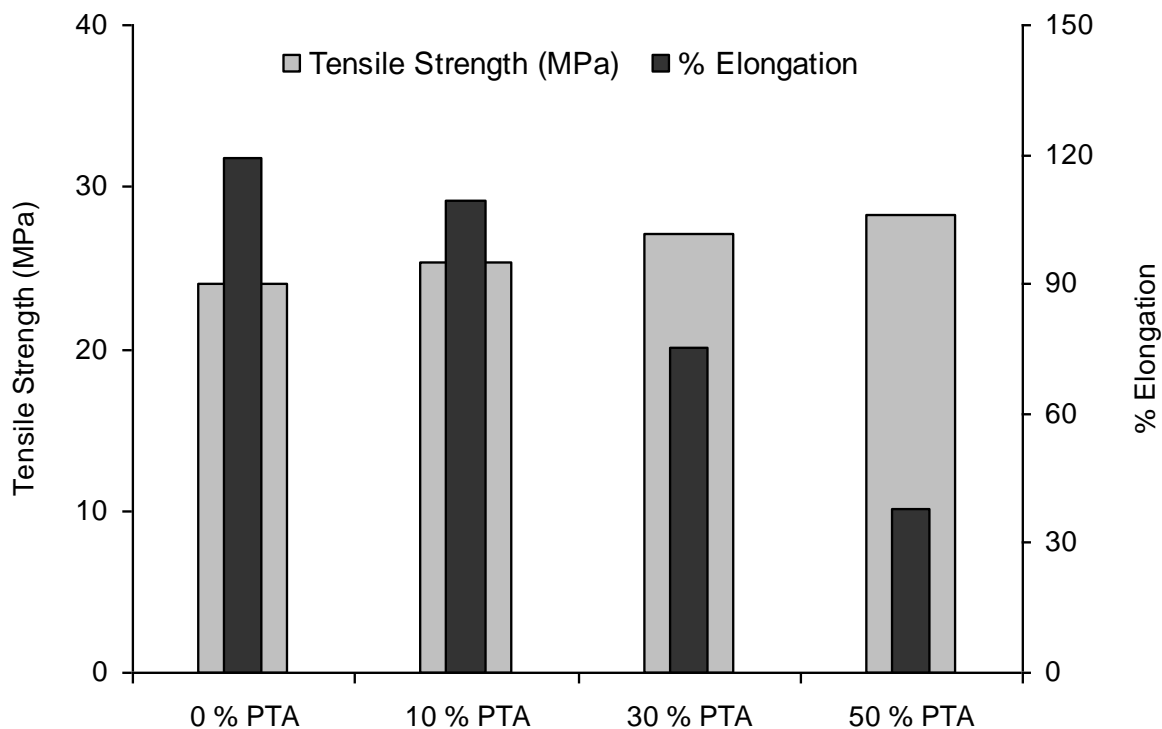
loss centered around 180 ^{o}C. This corresponds to weight loss of absorbed water, structural water associated with PTA and water as by-product by further esterification in the PVACO/PTA membranes. The second weight loss is centered around 250-450 ^{o}C is due to the thermal degradation of the ether and ester crosslinking linkages. The third weight loss is due to degradation of the polymer backbone which starts at around 600 ^{o}C. The crosslinked PVACO/PTA composite membranes show a considerably enhanced thermal stability than that of the pristine PVACO membrane.
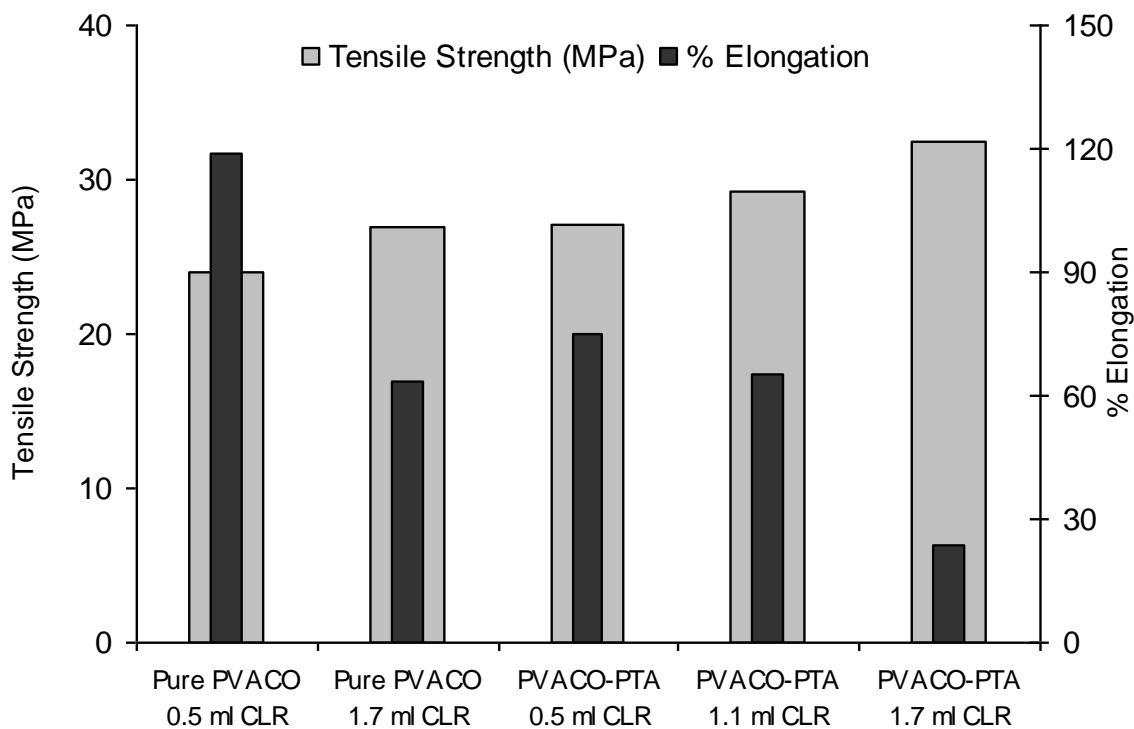

Figure 15. TGA thermograms of Pure PVACO (Uncrosslinked) & Crosslinked PVACO/PTA composite membranes with different wt. % PTA and GA CLR content

Table 2. Percent Weight Loss for the Pristine PVACO and the PVACO/PTA composite membranes

Membrane Details	30-200 ^{o}C	200-350 ^{o}C	350-700 ^{o}C	Residue (700 ^{o}C)
Pure PVACO	15 %	47 %	27 %	11 %
PVACO/30%PTA/0.5mlCLR	12 %	26 %	31 %	31 %
PVACO/30%PTA/1.7mlCLR	09 %	24 %	30 %	37 %
PVACO/50%PTA/0.5mlCLR	21 %	13 %	16 %	50 %

Figure 16. Mechanical properties of the Pristine PVACO and PVACO/PTA composite membranes with different PTA content and same CLR content of 0.5 ml
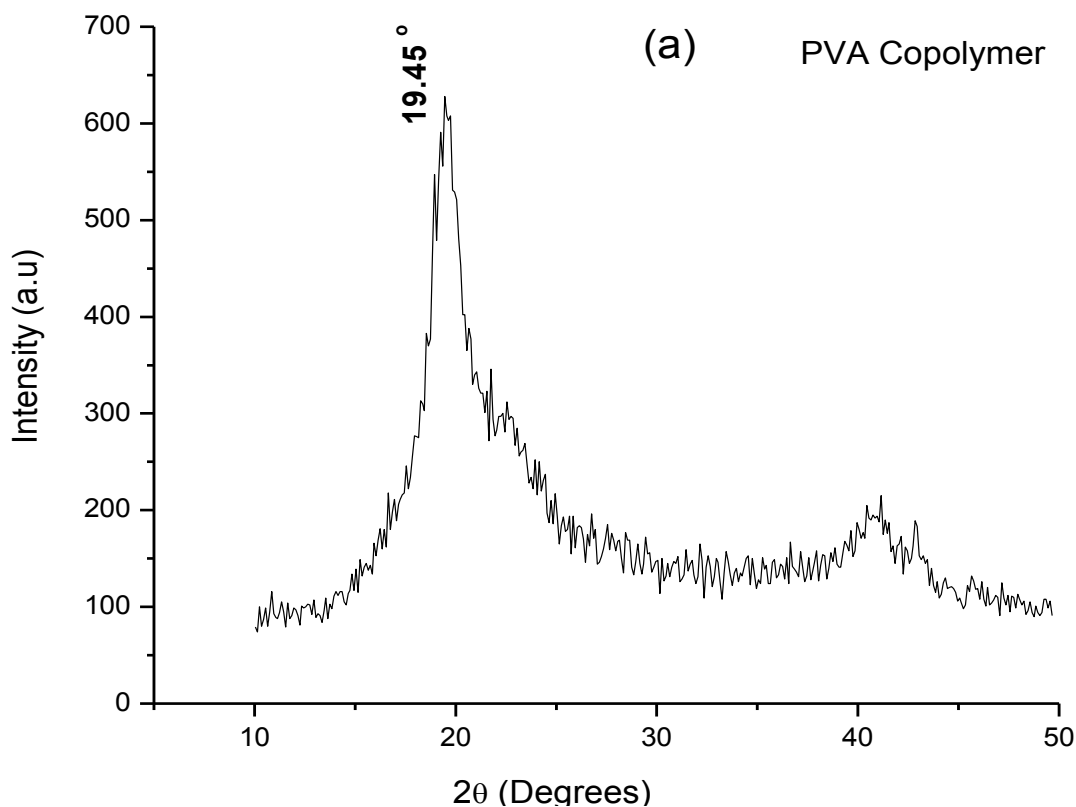

Figure 17. Mechanical properties of the Pristine PVACO and PVACO/PTA composite membranes with 30 wt. % PTA content and different CLR content

Tensile strength of 18 MPa and percent elongation of 430 % was observed for pristine PVACO membrane, when the PVACO membrane is crosslinked with glutaraldehyde the tensile strength for the pure crosslinked membranes increased with increase in CLR content whereas a reverse trend is observed for the percent elongation at break for these membranes.

The tensile strength and percent elongation at break for the PVACO/PTA composite membranes with different PTA content and cross-link density are shown in Fig. 16 and 17 respectively. The tensile strength for the composite membranes with different PTA content increases slightly with the incorporation of PTA and is further augmented with the increase in PTA content of the membrane. The percent elongation of the composite membranes is always lower than that of the pristine membranes with same crosslink density. Further the percent elongation of the composite membranes decreases with increase in acid content (PTA) of the membranes. This decrease in percent elongation can be due to the esterification of the hydroxyl groups of PVACO and hence resulting in reduction in the extent of hydrogen bonding between the hydroxyl groups of PVACO.

The tensile strength of the PVACO/PTA composite membranes with different CLR content increases with increase in CLR whereas the percent elongation at break decreases with increase in cross-link density of the membrane. From the results it can be observed that the crosslinked membranes exhibit higher tensile strength than the pristine PVACO membrane. This enhancement in tensile strength and decrease in percent elongation is due to the formation of crosslinked networks hence restricted mobility of the polymer chains.
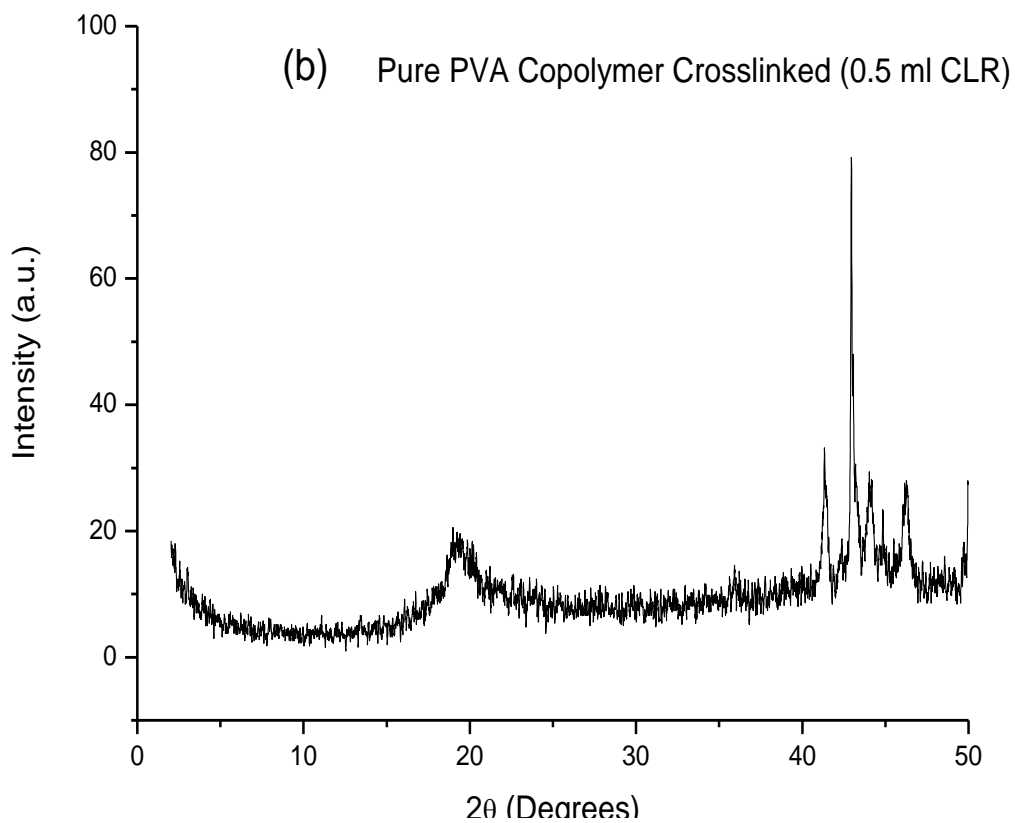
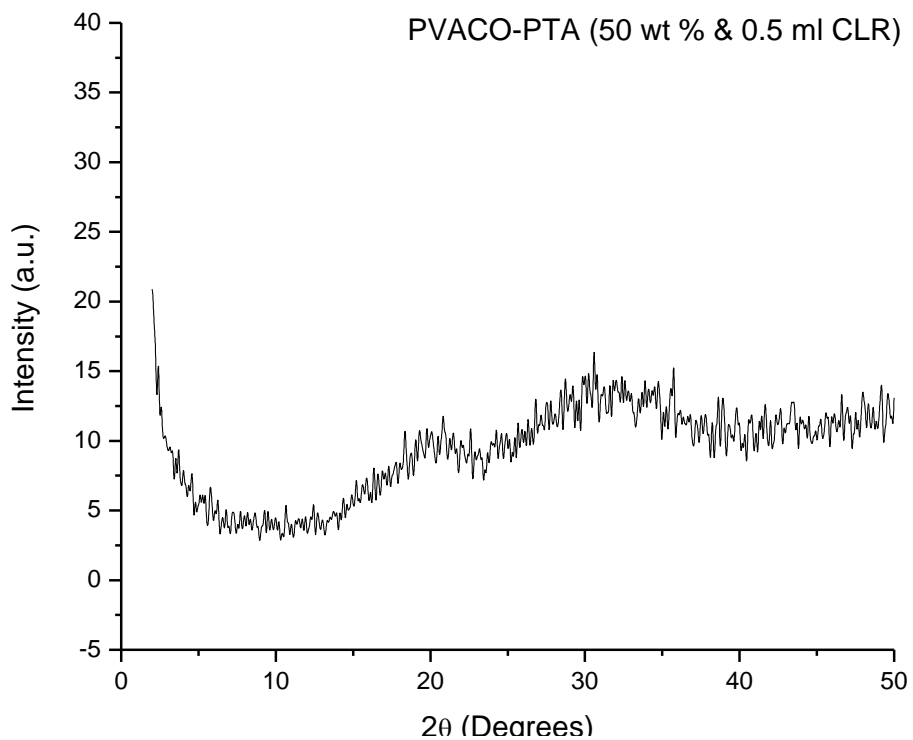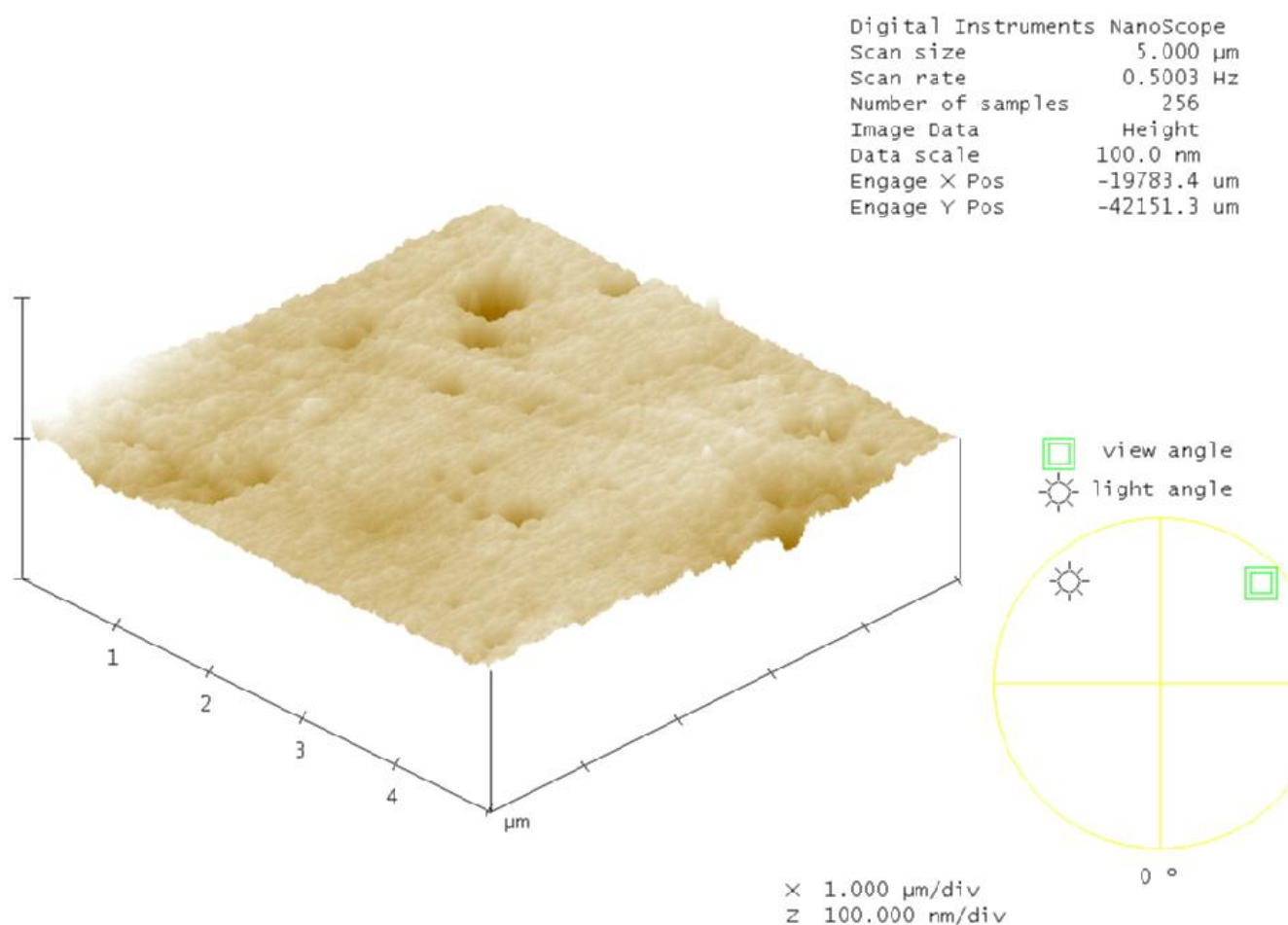**Figure 18.** X-ray Diffraction pattern of Pure PVACO (a) Un-Crosslinked (b) Crosslinked

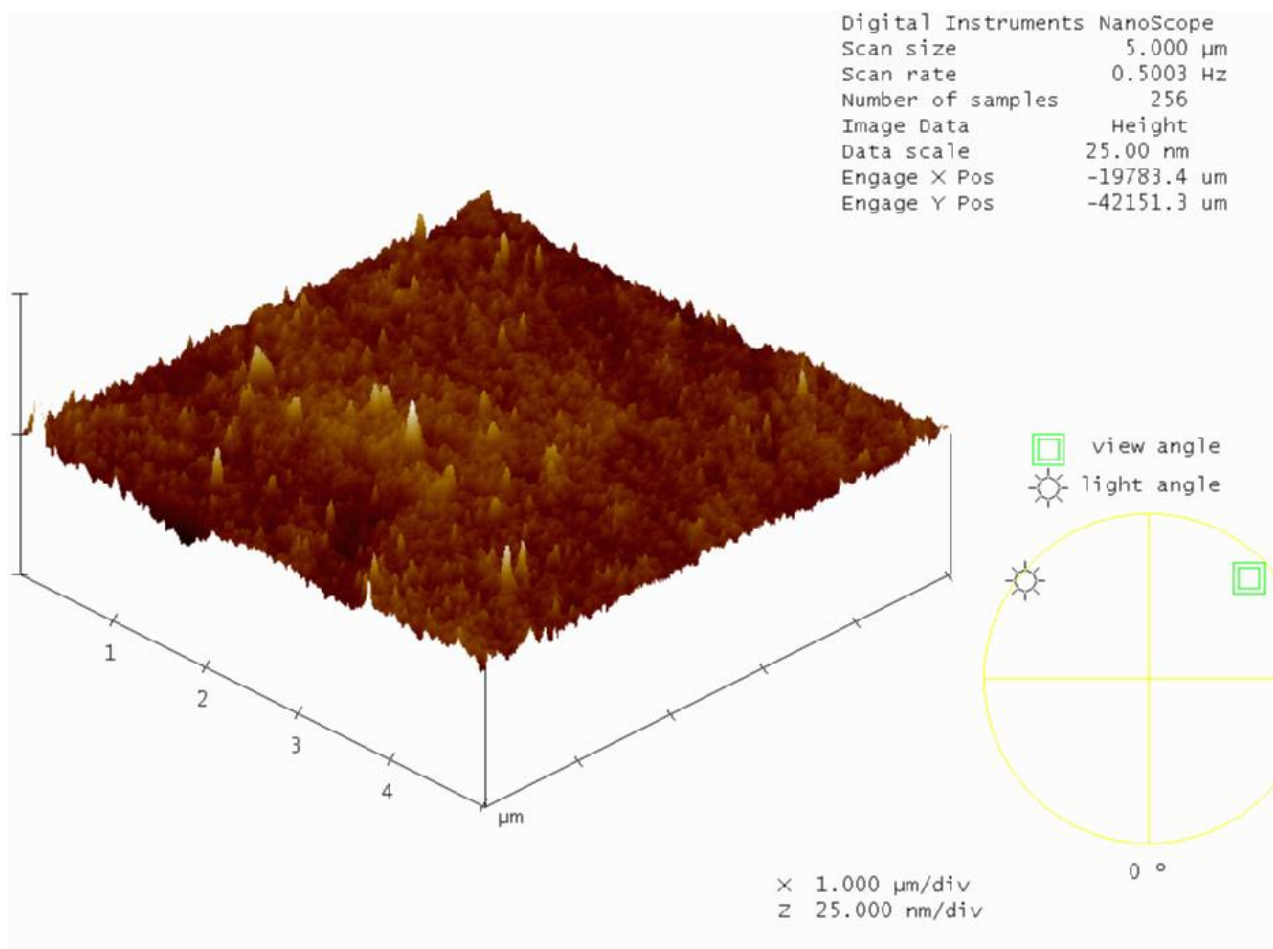**Figure19.** X-ray Diffraction pattern of PVACO-PTA Composite Membranes

X-ray diffraction analysis of pristine PVACO (uncrosslinked and crosslinked) and the PVACO/PTA composites membranes were performed. The XRD patterns for the uncrosslinked, crosslinked pristine PVACO as well as the PVACO/PTA composite membranes are depicted in Fig. 18 and Fig. 19. The range of the diffraction angle $2\theta = 2 - 50^{o}$. The crystallinity of the composite membranes is mainly due to PVACO. PVA is well known to exhibit a semi-crystalline structure with a large peak at a 2θ angle of $19–20^{o}$ and a small peak of $39–40^{o}$ [32] similarly a large peak at $2\theta = 19.45^{o}$ and a small peak at 41° was observed for the pure PVACO membranes as shown in Fig. 18(a). There is considerable broadening in the XRD peaks (Fig. 19) due to PVACO in the PVACO-PTA composite membranes. This feature indicates the reduction in the crystallinity of the composite membranes. The reduction in crystallinity of the composite membranes plays an important role in increasing the conductivity of the composite membranes.

Figure 20. Tapping Mode (3D) AFM images of pure uncrosslinked PVACO membrane

The surface morphology of the pure PVACO membranes and the PVACO/PTA composite membranes was analyzed by Tapping Mode - Atomic Force Microscopy (TM-AFM). Quantitatively, the differences in the morphology can be expressed in terms of various roughness parameters such as the mean roughness R_a, the root mean square (rms) of vertical data R_q, and the maximum height R_{max}. Here, the mean roughness is the mean value of surface relative to the center plane, the plane for which

the volume enclosed by the image above and below this plane are equal; R_{max} the height difference between the highest and lowest points on the surface relative to the mean plane and R_q is the standard deviation of the Z values within the given area. The roughness parameters were calculated for all membrane surfaces and have been summarized in Table 3.

Figure 21. Tapping Mode (3D) AFM images of pure crosslinked PVACO membrane (1.7 ml GA CLR)

Table 3. Roughness parameters for Pristine PVACO and PVACO/PTA composite membrane surfaces

Membrane Details	R_a (nm)	R_{max} (nm)	R_q (nm)
Pure PVACO (Uncrosslinked)	3.06	108.30	5.46
PVACO 1.7 ml CLR (0 % PTA)	0.73	15.45	0.97
30 % PTA 0.5 ml CLR	2.07	29.51	2.74
50 % PTA 0.5 ml CLR	23.06	343.22	31.09
30 % PTA 1.7 ml CLR	3.36	49.99	4.44

The TM-AFM images of the uncrosslinked and cross-linked pure PVACO membranes are depicted in Fig. 20 and 21 respectively. It can be realized by comparing the AFM images of 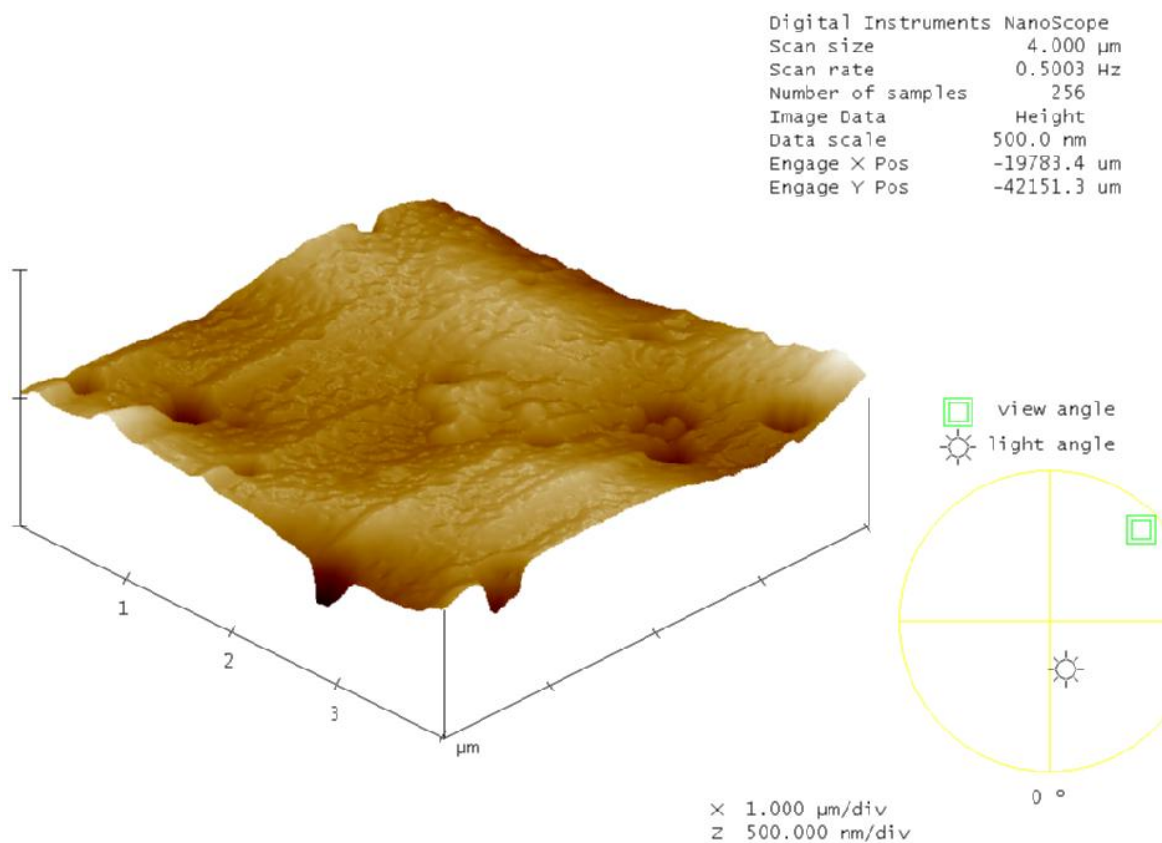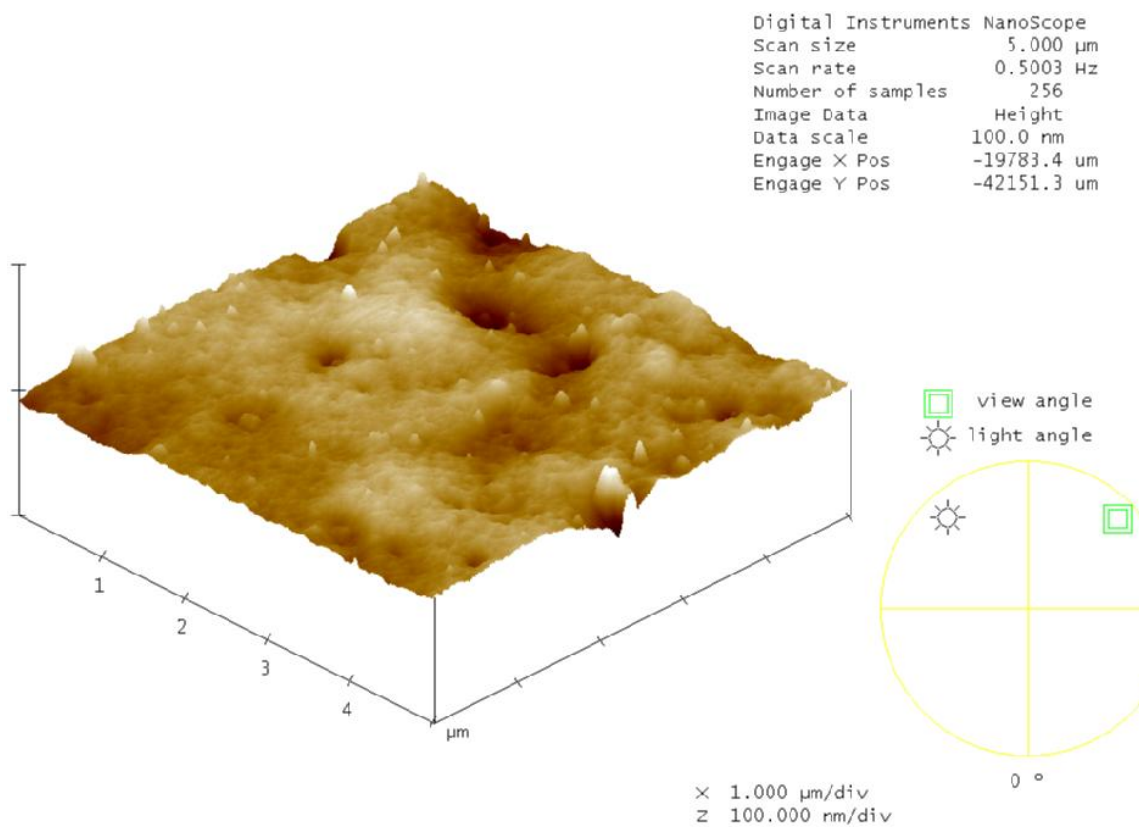different membranes that the morphology of the pure polymer surface changed significantly after cross-linking. The AFM images of uncrosslinked PVACO membrane shows a porous morphology (about 0.5 μm in diameter) and the mean roughness of 3.10 nm for the surface topography of the membrane, whereas the cross linked PVACO membrane with 1.7 ml CLR shows a homogeneous, non porous surface morphology and also a much smoother surface topography, mean roughness of 0.73 nm. The composite membrane with 30 wt. % PTA content (Fig. 22) shows a homogeneous and non-porous morphology but the surface morphology shows a substantial change with increase of PTA content of the composite membranes to 50 wt. % (Fig. 23). The mean roughness for the surface topography of the membrane increases from 2.07 nm to 23.06 nm with increase in PTA content of the composite membranes from 30 to 50 wt %. This shows that the phosphotungstic acid tends to form bigger aggregates with increase in the acid content of the composite membranes. When the crosslink density of the composite membrane with 30 wt. % PTA content is increased from 0.5 to 1.7 ml CLR (Fig. 24) then the mean roughness of the surface of the membrane increased from 2.07 nm to 3.36 nm.

Figure 22. Tapping Mode (3D) AFM images of PVACO-PTA composite (30 % PTA, 0.5 ml CLR)

Digital Instruments NanoScope
Scan size   4.000 µm
Scan rate   0.5003 Hz
Number of samples   256
Image Data   Height
Data scale   500.0 nm
Engage X Pos   -19783.4 um
Engage Y Pos   -42151.3 um

view angle
light angle

0 °

X 1.000 µm/div
Z 500.000 nm/div

Figure 23. Tapping Mode (3D) AFM images of PVACO-PTA composite (50 % PTA, 0.5 ml CLR)

Digital Instruments NanoScope
Scan size   5.000 µm
Scan rate   0.5003 Hz
Number of samples   256
Image Data   Height
Data scale   100.0 nm
Engage X Pos   -19783.4 um
Engage Y Pos   -42151.3 um

view angle
light angle

0 °

X 1.000 µm/div
Z 100.000 nm/div

Figure 24. Tapping Mode (3D) AFM images of PVACO-PTA composite (30 % PTA, 1.7 ml CLR)

Hyder et al. [33,34] reported that the roughness of crosslinked PVA membranes was more than the uncrosslinked membranes whereas we observed that the surface roughness of the pristine PVACO membranes decreased when crosslinked with glutaraldehyde, a slight increase in the surface roughness was observed with increase in crosslinking for the composite membranes. These two different observations can be attributed to approach utilized for accomplishing the crosslinking reaction, we utilized in situ solution crosslinking during the preparation of the membranes which was expected to produce uniform crosslinking throughout the membrane whereas Hyder et al. crosslinked the membranes by utilizing a crosslinking solution after membrane preparation which will tend to result in a non uniform crosslinking across the cross section of the membrane with highest crosslinking at the surface which leads to the increase in roughness of these membrane surfaces.

4. CONCLUSION

This work reports the fabrication and characterization of PVACO-PTA based crosslinked composites by various characterization techniques. The FTIR studies confirmed the formation of crosslinked networks and the occurrence of strong interaction of the heteropoly acids with the hydroxyl and carboxylic acid groups of the PVACO polymer matrix through the terminal and bridging oxygen atoms, which helps in immobilizing the PTA in the PVACO polymer matrix. The water uptake and the dopant loss from the composite membranes can be controlled by optimizing the PTA content and the crosslink density of the composite membranes. The optimum membrane property among the PVACO-PTA composites was observed for the membrane with 50 wt. % PTA and 0.5 ml GA CLR, a conductivity of 2.3×10^{-3} S/cm and a methanol permeability of 3.35×10^{-6} cm^2/s was observed for this PEM. The variation in conductivity with temperature follows an Arrhenius relationship and the values of activation energy for proton conduction in the PVACO-PTA composite membranes ranges between 0.13 -0.17 eV as determined from the Arrhenius plots. Improvement in thermal and mechanical properties of the PVACO-PTA composites was observed with the incorporation of PTA in the PVACO polymer matrix and crosslinking of the polymer matrix respectively. X-Ray diffraction studies showed decrease in crystallinity of the composite membranes which plays an important role in enhancing the proton conductivity of the composite membranes. All the PVACO-PTA composite membranes showed very smooth surface morphology as observed by the AFM except for the composite membrane with the highest (50 wt %) acid content.

References

1. R. F. Service, *Science*, 296 (2002) 1222
2. C. C. Yang, Y. J. Lee and J. M. Yang, *J. Power Sources*, 188 (2009) 30

3. C. C. Yang and Y. J. Lee, *Thin Solid Films*, 517 (2009) 4735
4. J. W. Rhim and Y. K. Kim, *J. Appl. Polym. Sci.*, 75 (2000) 1699
5. W. Y. Chiang and C. L. Chen, *Polymer*, 39 (1998) 2227
6. G. G. Kumar, P. Uthirakumar, K. S. Nahm and R. N. Elizabeth, *Solid State Ionics*, 180 (2009) 282
7. J. W. Rhim, H. B. Park, C. S. Lee, J. H. Jun, D. S. Kim and Y. M. Lee, *J. Memb. Sci.*, 238 (2004) 143
8. T. Yang, Q. Xu, Y. Wang, B. Lu and P. Zhang, *Int. J. Hydrogen. Energy*, 33 (2008) 1014
9. T. Yang, *Int. J. Hydrogen. Energy*, 33 (2008) 6772
10. A.K. Sahu, G. Selvarani, S. D. Bhat, S. Pitchumani, P. Sridhar, A. K. Shukla, N. Narayanan, A. Banerjee and N. Chandrakumar, *J. Memb. Sci.*, 319 (2008) 298
11. K. Y. Lee, N. Mizuno, T. Okuhara and M. Misono, *Bull. Chem. Soc. Jpn.*, 62 (1989) 1731
12. B. B. Bardin, S. V. Bordawekar, M. Neurock and R.J. Davis, *J. Phys. Chem. B,* 102 (1998) 10817
13. K. D. Kreuer, *Chem. Mater.*, 8 (1996) 610
14. G. M. Haugen, F. Meng, N. V. Aieta, J. L. Horan, M. C. Kuo, M. H. Frey, S. J. Hamrock and A. M. Herring, *Electrochem. Solid State Lett.*, 10 (2007) B51
15. V. Ramani, H. R. Kunz and J. M. Fenton, *J. Membr. Sci.*, 266 (2005) 110
16. V. Ramani, H. R. Kunz and J. M. Fenton, *J. Power Sources*, 152 (2005) 182
17. V. Ramani, H. R. Kunz and J. M. Fenton, *Electrochim. Acta*, 50 (2005) 1181
18. P. Staiti and M. Minutoliv, *J. Power Sources*, 94 (2001) 9
19. A.Anis, A. K. Banthia, S. Mondal and A. K. Thakur, *Chinese Journal of Polymer Science*, 24 (2006) 449
20. A.Anis, A. K. Banthia and S. Bandyopadhyay, *J. Materials Engineering and Performance*, 17 (2008) 772
21. A.Anis, A. K. Banthia and S. Bandyopadhyay, *J. of Power Sources*, 179 (2008) 69
22. L. M. G. Sainero, S. Damyanova and J. L. G. Fierro, *Appl. Catal. A: General*, 208 (2001) 63
23. Noto V. Di, M. Vittadello, V. Zago, G. Pace and M. Vidali, *Electrochim. Acta*, 51 (2006) 1602
24. M. V. Fedkin, X. Zhou, M. A. Hofmann, E. Chalkova, J. A. Weston, H. R. Allcock and S. N. Lvov, *Materials Letters,* 52 (2002) 192
25. *ASTM – D – 638*: Standard Test Method for Tensile Properties of Thin Plastic Sheeting
26. C. Rocchiccioli-Deltcheff, M. Fournier, R. Franck and R. Thouvenot, *Inorg. Chem.*, 22 (1983) 207
27. H. Gao, Q. Tian and K. Lian, *Solid State Ionics*, 181 (2010) 874
28. S. Guhan, N. A. Kumar and D. Sangeetha, *Chinese Journal of Polymer Science,* 27 (2009) 157
29. U. Thanganathan, J. Parrondo and B. Rambabu, *J Appl Electrochem*, 41 (2011) 617
30. A.Anis and A. K. Banthia, *Materials and Manufacturing Processes,* 22 (2007) 737
31. Y. Zhang, Z. Cui, C. Liu, W. Xing and J. Zhang, *J. Power Sources*, 194 (2009) 730
32. C. C. Yang, S. J. Chiu and C.T. Lin, *Journal of Power Sources*, 177 (2008) 40
33. M. N. Hyder, R. Y. M. Huang and P. Chen, *Journal of Membrane Science*, 283 (2006) 281
34. M. N. Hyder, R. Y. M. Huang and P. Chen, *Journal of Membrane Science*, 326 (2009) 363